THE LIGHT GREEN PHENOTYPE 1 PROTEIN IS REQUIRED FOR PHOTOSYSTEM I-LIGHT HARVESTING COMPLEX ASSEMBLY IN *CHLAMYDOMONAS REINHARDTII*

A Thesis Submitted to the
College of Graduate and Postdoctoral Studies
In Partial Fulfillment of the Requirements
For the Degree of Master of Science
In the Department of Biology
University of Saskatchewan
Saskatoon

By

Carmen Marquez Mellidez

PERMISSION TO USE

In presenting this thesis/dissertation in partial fulfillment of the requirements for a Postgraduate degree from the University of Saskatchewan, I agree that the Libraries of this University may make it freely available for inspection. I further agree that permission for copying of this thesis/dissertation in any manner, in whole or in part, for scholarly purposes may be granted by the professor or professors who supervised my thesis/dissertation work or, in their absence, by the Head of the Department or the Dean of the College in which my thesis work was done. It is understood that any copying or publication or use of this thesis/dissertation or parts thereof for financial gain shall not be allowed without my written permission. It is also understood that due recognition shall be given to me and to the University of Saskatchewan in any scholarly use which may be made of any material in my thesis/dissertation.

DISCLAIMER

Reference in this thesis/dissertation to any specific commercial products, process, or service by trade name, trademark, manufacturer, or otherwise, does not constitute or imply its endorsement, recommendation, or favoring by the University of Saskatchewan. The views and opinions of the author expressed herein do not state or reflect those of the University of Saskatchewan and shall not be used for advertising or product endorsement purposes.

Requests for permission to copy or to make other uses of materials in this thesis/dissertation in whole or part should be addressed to:

Head of the Department of Biology

112 Science Place

University of Saskatchewan

Saskatoon, Saskatchewan S7N 5E2

Canada

OR

Dean

College of Graduate and Postdoctoral Studies

University of Saskatchewan

116 Thorvaldson Building, 110 Science Place

Saskatoon, Saskatchewan S7N 5C9

Canada

ABSTRACT

In the green alga *Chlamydomonas reinhardtii*, the light harvesting (LHC) proteins form a dynamic complex that regulates the amount of light energy being absorbed by the cell and transmitted to the photosynthetic reaction centers. Because resonance energy transfer efficiency declines with distance between chlorophyll molecules, the organization of the LHC proteins is critical for the process of energy transmission. Studies have suggested that LHC organization requires the assistance of chaperone-type assembly factors, but to date none have been identified. In this study we used a high-light sensitive *psaF* mutant to identify a LHC assembly-factor candidate. The mutant identified had a light green phenotype (*lgp1*). The cells accumulate approximately 66% of wild-type chlorophyll levels, with an elevated Chl a/b, suggesting LHC abundance. Steady-state chlorophyll fluorescence measurements suggest a moderate impact on photosynthetic function with a decline in electron flow from PSII to PSI. A semi-quantitative assessment of individual LHC subunits found that all LHC proteins accumulated at lower levels except for LHCA8, LHCB2 and LHCBM5. By Blue-Native Gel (BN) electrophoresis, it was discovered that high molecular weight PSII-LHC complexes were missing in *lgp1*. This was confirmed using 2D-PAGE. Our introductory analysis suggests that the LGP1 protein is involved in connecting specific LHC proteins to PSII. We are working to confirm this by examining protein-protein interactions between LGP1, PSII, and the diminished LHC proteins. If confirmed, LGP1 would be the first LHC assembly-factor identified in *C. reinhardtii*.

ACKNOWLEDGEMENTS

I would first like to thank my thesis advisor Dr. Kenneth E. Wilson of the Biology Department at University of Saskatchewan. The door to Prof. Wilson's office was always open whenever I ran into a trouble spot or had a question about my research or writing. He consistently allowed this paper to be my own work but steered me in the right the direction whenever he thought I needed it.

I would also like to thank the experts who were involved in my committee for this research project: Dr. Peta Bonham-Smith and Dr. Yangdou Wei. Without their participation and valuable input, my whole research activity could not have been successfully conducted.

I would also like to acknowledge Dr. Ewa Miskiewicz for being an invaluable asset in the laboratory techniques, and I am gratefully indebted to her for her very valuable comments and full support on this research and thesis.

Finally, I must express my very profound gratitude to my parents and to my husband for providing me with unfailing support and continuous encouragement throughout my years of study and through the process of researching and writing this thesis. This accomplishment would not have been possible without them. Thank you.

TABLE OF CONTENTS

LIST OF FIGURES

LIST OF TABLES

LIST OF ABREVIATIONS

2D	Two dimensional
BAC	Bacterial artificial chromosome
BN (G)	Blue native gel
BP	Base pairs
C. reinhardtii	*Chlamydomonas reinhardtii*
Chl a	Chlorophyll a
Chl b	Chlorophyll b
Chl a/Chl b	Chlorophyll a to b ratio
CUGI	Clemson University Genomics Institute
DH5-α	High efficiency NEB 5-α competent *E. coli*
DNA	Deoxyribonucleic acid
DPOR	Light independent proto-chlorophyllide oxidoreductase
E. coli	*Escherichia coli*
fmols	Femtomoles
g	Acceleration = gravity
kDa	Kilo daltons
LB	Luria broth
LHC	Light Harvesting Complexes
M	Molar
MIN	Minutes
mL	Millilitres
mM	Millimolar
nm	Nanometer
PAGE	Polyacrylamide gel electrophoresis
pCM010	pLM006 plasmid that contains the suggested *LGP1* gene
PCR	Polymerase chain reaction
pLM006	Plasmid with RFP-His tag, PSAD-driven promoter (Mackinder et al., 2017)
pmol	Picomoles
PSAD	Subunit D present in the core of Photosystem I

PSAF	Subunit F present in the core of Photosystem I
PSBB	Subunit B present in the core of Photosystem II
PSBC	Subunit C present in the core of Photosystem II
PSI	Photosystem I
PSII	Photosystem II
PVDF	Polyvinylidene difluoride
RC	Reaction centre
RESDA-PCR	Restriction enzyme site-directed amplification
RFP	Red fluorescence protein
ROI	Region of interest
RT	Room temperature
RT-PCR	Real time polymerase chain reaction
SDS	Sodium dodecyl sulfate
TAP	Tris-acetate-phosphate media
TBST	Tris buffered saline with tween
Tris-min	Tris-minimal media
µg	Micrograms
µL	Microlitres
V	Volts

CHAPTER 1

1. INTRODUCTION

Photoautotroph organisms can face serious and sometimes, irreparable damage when exposed to levels of light energy that are in excess of their needs for growth and metabolism (Erickson et al., 2015; Taiz et al., 2015). Considering this energy balance, when cells are exposed to more light energy than they can use, energy absorbed by the photosynthetic system can result in damage to the cell. For example, toxic molecules such as superoxide, singlet oxygen, and peroxides - collectively known as reactive oxygen species (ROS) - are produced. Under extreme conditions, ROS can trigger programmed cell death in plants, or simply overwhelm cellular defences and damage cells beyond repair (Taiz et al., 2015). Because plants have evolved in fluctuating environments where light levels can change on the time scale of seconds to the annual change of seasons, they have many mechanisms to protect themselves. Understanding the protective systems of the photosynthetic apparatus has been an ongoing study since the early 1960s. Research has focused on many aspects, from plant developmental processes that regulate stem length and leaf thickness to protein conformational changes that regulate light absorption at the sub-second level (Hawes and Satiat-Jeunemaitre, 2001). Somewhat ironically, my thesis uses light induced cell death in the green alga *Chlamydomonas reinhardtii* as a tool to study the protection of Photosystem I from excess light.

1.1. Introduction to photosynthesis

Life on earth depends ultimately on the energy derived from the sun and photosynthetic organisms are the only ones that can harvest this energy. These organisms are able to use solar energy to synthesize carbohydrates and generate oxygen from carbon dioxide and water. Photoautotroph organisms such as most plants, algae and cyanobacteria perform photosynthesis as part of their life cycle (Hawes and Satiat-Jeunemaitre, 2001; Taiz et al., 2015).

In most plants and green algae, photosynthesis is carried out in the chloroplast(s). These organelles have a very intricate but highly efficient system of internal membranes known as thylakoids, in which the energy collecting photosynthetic apparatus is embedded (Harris, 2008). The conversion of light into a usable form of chemical energy begins with the chlorophylls present in the thylakoid membrane , that are the primary absorbers of the light energy required for photosynthesis (Figure 1.1). Nearly all chlorophyll molecules in the photosynthetic apparatus have a light-gathering or antenna function and they act as the primary acceptors of electromagnetic radiation (Taiz et al., 2015).

The study of the light responses in photosynthetic organisms led researchers in the early 1960s to discover and define the photochemical complexes, Photosystem I (PSI) and Photosystem II (PSII). The photosynthetic unit is composed of the photoreaction center, the corresponding antenna chlorophylls (P680 in Photosystem I and P700 in Photosystem II), the auxiliary pigment/protein complexes and the electron transport chain (Figure 1.1). The antenna complexes, the Light Harvesting Complexes (LHC), are believed to surround the Reaction Centres (RC) in both photosystems (Figure 1.2 and Figure 1.3). The LHC have a dual role. They greatly increase the amount of light and range of wavelengths that are collected for use by the reaction centre. They also help to protect the reaction centre when unfavourable light conditions occur (Figure 1.2 and Figure 1.3). There exist structural differences in vivo between how the LHC are inserted in each photosystem, as depicted in Figure 1.2 and Figure 1.3. Crystallography models obtained from higher plants have confirmed that the RC in both PS are bound to the thylakoid membrane by transmembrane protein helices, whereas the chlorophyll molecules are bound by histidine residues with the nonheme iron present in the RC (Ort and Yocum, 1996; Su et al., 2019). Whereas in Photosystem I its LHC form an arc surrounding its RC (Figure 1.2) (Suga et al., 2019), the proposed structure present in Photosystem II is believed to have four main complexes closely organized to protect the RC (Figure 1.3) (Sheng et al., 2019). In *Chlamydomonas reinhardtii*, the PSII shows different stoichiometric relationships with its LHC, as depicted in Figure 1.3. The LHCII are organised in different super complexes including the $C_2S_2M_2L_2$, which is the largest super complex in PSII defined to date (Sheng et al., 2019). The C_2S_2 particle is essentially a dimer containing two copies each of PSII reaction centre core, CP26, CP29, and an LHCII trimer (Iwai et al., 2008; Nield et al., 2000). These photosystems are believed to be organized as shown in Figure 1.4, where there exists a spatial separation between

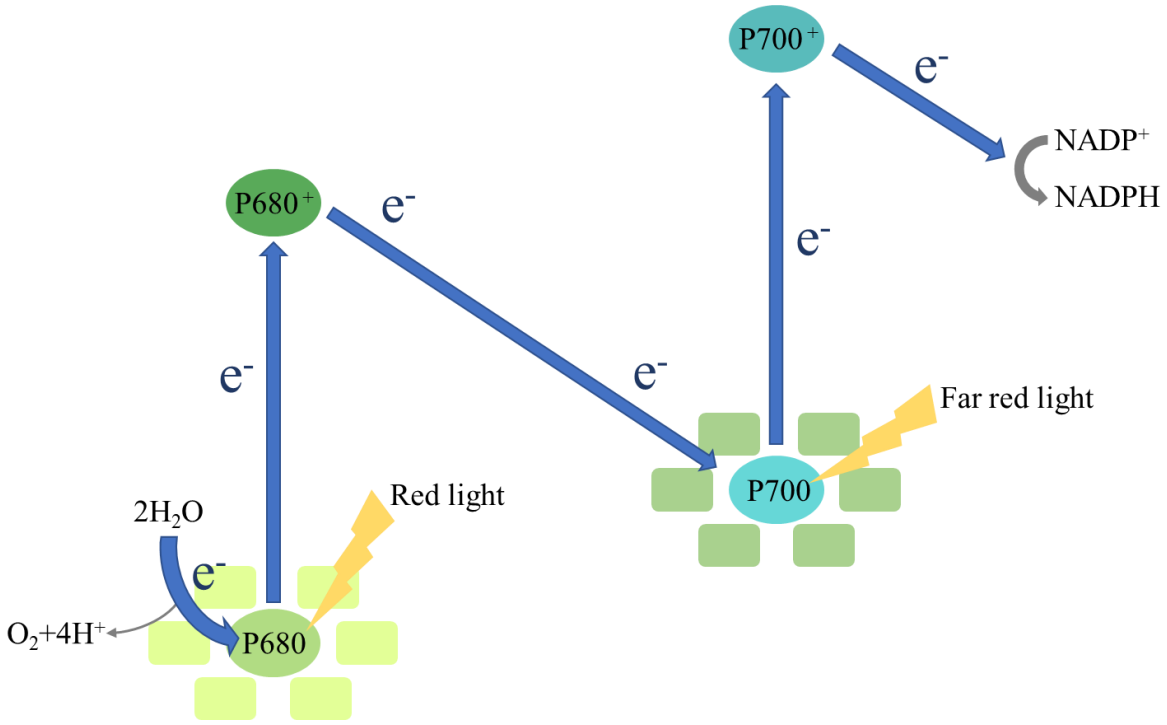

Figure 1.1. Z-scheme diagram representing the electron transport chain occurring in the light reactions in photosynthesis. P680 is the special pair of chlorophyll molecules at the heart of the Photosystem II reaction centre (RC) while P700 is the chlorophyll pair at the centre of Photosystem I. As a photon of light is absorbed by PSII and transferred to P680, an electron of the special pair is excited to create $P680^{*}$ before the electron is transferred to the electron transport chain, producing $P680^{+}$. As this process continues electrons are sequentially taken away from two water molecules providing four electrons to replace those transferred from P680 into the electron transport chain. This process releases $4H^{+}$ into the thylakoid lumen and produces one O_2 molecule, as a by-product. Electrons in the transport chain are transferred to P700 by plastocyanin via the quinone-cytochrome b_6f complex. Upon excitation of P700 to $P700^{*}$ an electron is transferred to $NADP^{+}$ producing NADPH. P700 is regenerated by the electrons originating from H_2O. Two cycles of P700 oxidation and reduction converts $NADP^{+}$ to NADPH. This process is called linear electron transport as the electrons move from H_2O to $NADP^{+}$.

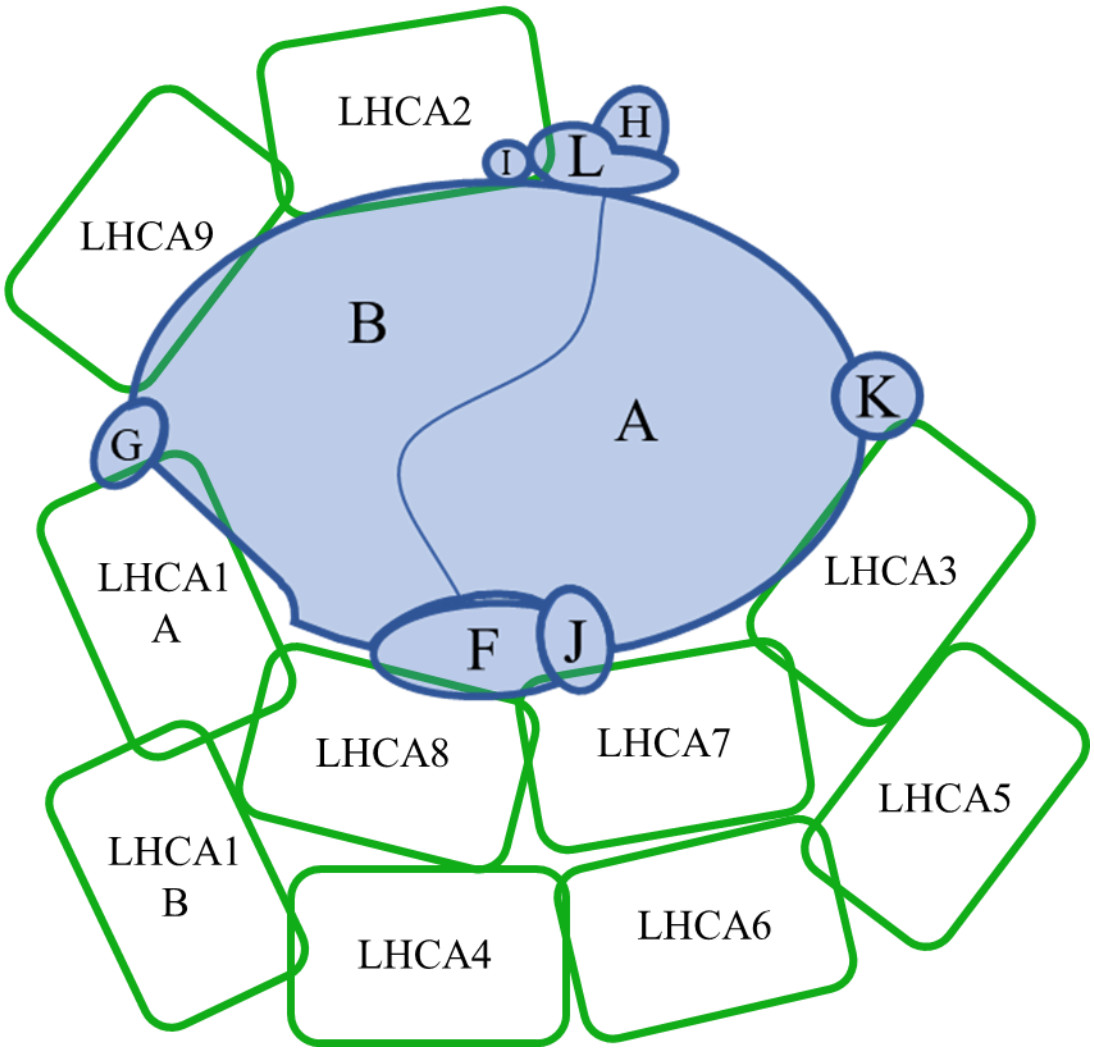

Figure 1.2. Proposed distribution of Light Harvesting Complexes surrounding the reaction centre in Photosystem I in *Chlamydomonas reinhardtii* cells. The LHCA proteins (in green) form an arc surrounding the PSI reaction centre (blue). Key PSI subunits known to interact with LHCA proteins are shown and denoted by their subunit letter (would be *PSAA, PSAB, PSAF, PSAG, PSAH, PSAI, PSAJ, PSAK and PSAL*). This figure is redrawn based on work presented in (Suga et al., 2019).

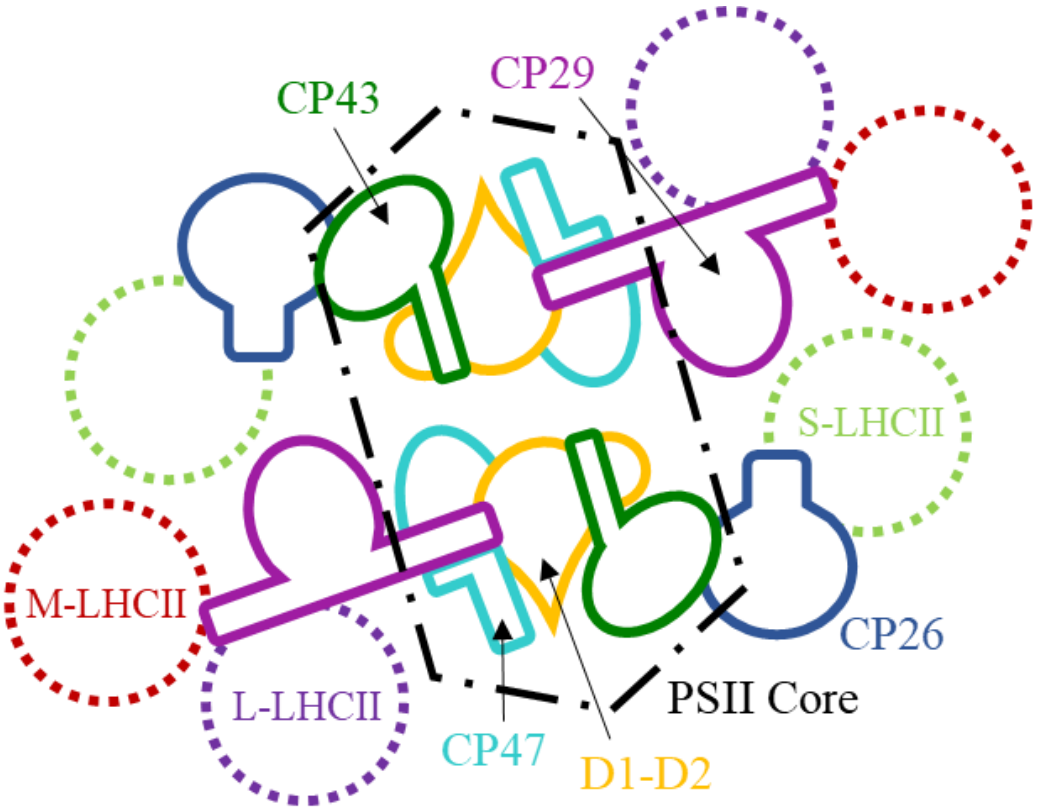

Figure 1.3. Proposed structural distribution of Light Harvesting Complexes surrounding the reaction centre in algal Photosystem II. The LHCB proteins form a belt surrounding the PSII reaction centre (black dotted line). Four main LHCII super complexes are highlighted in the picture: CP26 (LHCB5), CP29 (LHCB4), CP43 (PSBC) and CP47 (PSBB). The dotted circles represent the associated PSII-LHCII trimers: S-LHCII (strongly), M-LHCII (moderately), and L-LHCII (loosely) associated complexes. This figure is redrawn based on work presented in (Sheng et al., 2019).

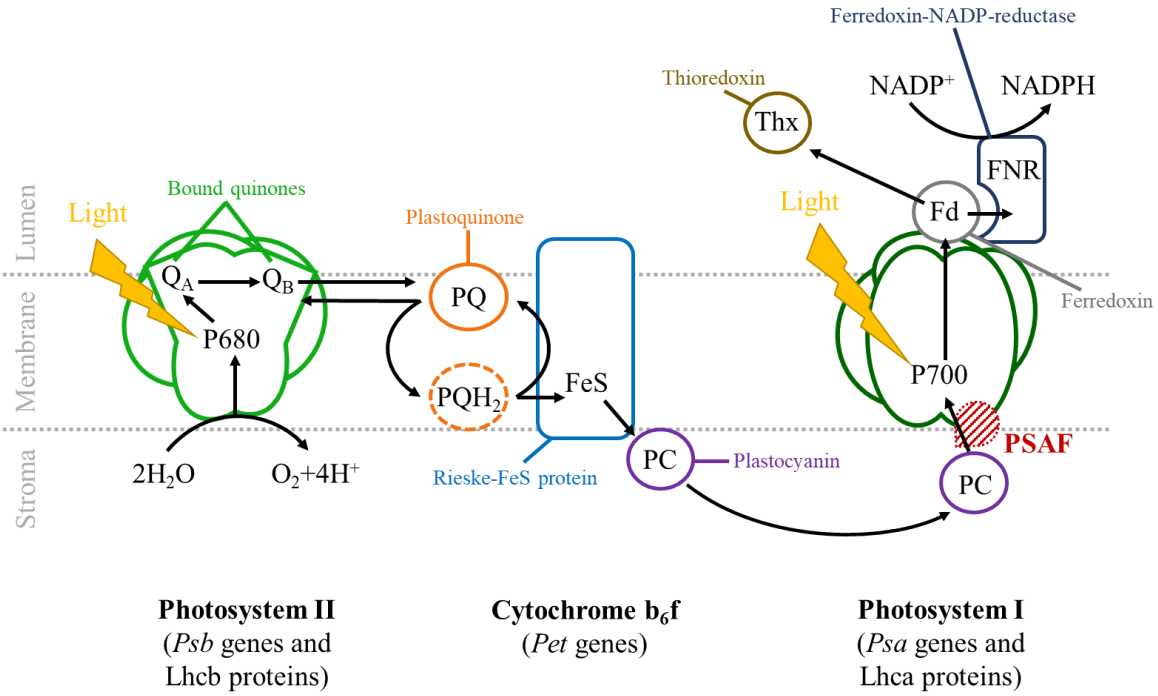

Figure 1.4. A linear depiction of the photosynthetic electron transport chain of *C. reinhardtii*. The path of electron movement is represented by bold black arrows. The electrons originate from the photolysis of two water molecules and end up with the reduction of $NADP^+$ to NADPH. The PSAF subunit of Photosystem I is highlighted in red, it provides a docking site for Plastocyanin (PC). In the absence of the PSAF subunit, electron transfer from PC to P700 is slow. Under conditions of excess excitation, this donor-side limitation results in the production of reactive oxygen species and ultimately the death of the cell. This figure is redrawn based on work presented in (Wilson et al., 2006).

both PS forcing two diffusible carriers, plastoquinone (PQ) and plastocyanin (PC), to deliver electrons from PSII to PSI. This separation leads to diffusion limited transport problems, but the separation of the light reactions into two parts allows the electron to be excited to a greater energy level than if a single photon was used. A second major benefit of the electron transport chain is the movement of H^+ ions across the thylakoid membrane. The use of light energy to move the H^+ ions generates a proton motive force (a form of potential energy) that is used by the ATP synthase to produce ATP, the second form of chemical energy needed to fix carbon dioxide (Taiz et al., 2015; Wilson et al., 2006).

As we have learned more about how the photosynthetic complexes interact and transfer energy to each other, we began to realize that the linear, separated system depicted in Figure 1.3 does not reflect what is occurring in the thylakoid membrane (Järvi et al., 2011; Rantala et al., 2017).

1.2. *Chlamydomonas reinhardtii* as a model to study photosynthetic protein complex assembly

C. reinhardtii is a unicellular, biflagellate green alga used as a model organism for studying processes such as organelle biogenesis and genetics, mating reactions and gametogenesis, and the assembly and operation of the photosynthetic apparatus (Harris, 2008). The term “green yeast” has been used in multiple reviews to describe *C. reinhardtii* (Goodenough, 1992; Rochaix, 1995). Like the yeast *Saccharomyces cerevisiae*, it has a fast growth rate (2 to 3 divisions per day) and it is haploid during vegetative growth, but it has two genetically controlled mating types. Gametogenesis can be induced in the lab by nitrogen starvation. Thus, it can be crossed to examine phenotype inheritance via tetrad analysis. This serves as an advantage when performing laboratory mutagenic studies, because with the cells being haploid during the vegetative stage, they show any potential phenotypes right away. This makes mutant generation and characterization much faster and easier than in diploid or polyploid higher plants (Grossman et al., 2003).

Studying photosynthetic mutants in *C. reinhardtii* is more easily done than in Arabidopsis because its photosynthetic function is dispensable (Dent et al., 2015). Thus *C. reinhardtii* is a facultative autotroph meaning it can grow photoautotrophically with CO_2 as a source, or it can grow non-photosynthetically with acetate as the main carbon source in its

growth medium. Being able to completely disrupt photosynthesis is one of the main reasons for the choice of *C. reinhardtii* as a research model organism (Harris, 2008). Having non-photosynthetic growth in the presence of acetate becomes essential when studying photosynthesis, as light-sensitive mutants can be isolated and used to better understand key factors such as electron carriers inside the photosynthetic electron transport chain (Gorman and Levine, 1965) or key proteins involved in state transitions such as the STT7 kinase (Berry et al., 2011; Depege et al., 2003). In fact, the work described by Depege et al. (2003) capped a 30-year search for the LHCII kinase (Allen, 2003). The classic genetic approach employed highlights the strength of this approach when a clear phenotype can be followed during a mutagenic study. It is in this type of forward genetic approach that *C. reinhardtii* shines as a model organism for the study of photosynthesis.

With any model organism, a key factor is a well described physiology, and ease of use. In *C. reinhardtii*, all three autonomous genetic systems located in the nucleus, chloroplast, and mitochondria, have well defined genetics. The three genomes have been sequenced and can be transformed using foreign DNA (Harris, 2008). When nuclear transformations of *C. reinhardtii* are studied, insertion of the transforming DNA into the nuclear genome occurs randomly. This property has been used successfully for disrupting genes involved in flagellar synthesis and photosynthesis (Li et al., 2000). In both cases, the genomic sequences flanking the transformation vector were used to map the insert to the genomic sequence. Molecular tools for manipulating *C. reinhardtii* normally use cell wall-deficient strains (Kindle, 1990). Cells carrying the *cw15* mutation can be efficiently transformed by agitation with DNA and glass beads, although electroporation techniques are generally more effective. Some of the biggest advances over the past 20 years fit in the ever-expanding molecular tool kit.

1.3. Photoprotection strategies in *C. reinhardtii*

C. reinhardtii has several photoprotective strategies when light conditions are unfavourable, as shown in Figure 1.5 (Erickson et al., 2015). As a motile organism, *C. reinhardtii*'s first response to damaging light conditions is moving away from the light source, a process known as negative phototaxis. Chloroplasts can alter their energetic state by changing the rate of electron transport or accumulating the PQ pool in a more reduced state. At the membrane level, carotenoids and xanthophylls play an essential role in photoprotection as the

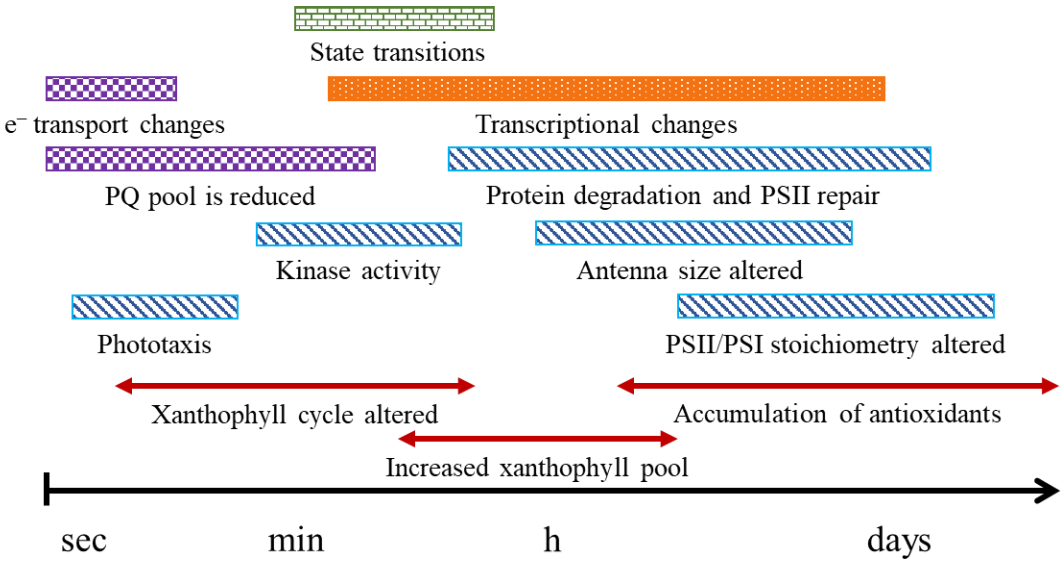

Figure 1.5. The time scale of effectiveness of photoprotective strategies utilized by *C. reinhardtii*. Non-photochemical quenching responses are shown in green (state transitions). Transcriptional changes (up-regulation of stress-response genes) are highlighted in orange. Changes in the chloroplast energetic state are shown in purple (electron transport chain changes and reduction of the plastoquinone pool). Protein activity and expression changes (kinase activity, PSII repair, phototaxis) are highlighted in blue, and variations in pigment accumulation and properties are shown by red arrows. This figure is redrawn based on work presented in (Erickson et al., 2015).

photosynthetic membrane can be easily damaged if the energy absorbed by chlorophyll cannot be used for photosynthesis. Carotenoids absorb light and are reactive oxygen scavengers. Under low light Violaxanthin (a xanthophyll cycle pigment) transfers energy to chlorophyll - under higher light levels as the H^+ gradient increases - violaxanthin gets converted to zeaxanthin, a compound that absorbs light energy from chlorophyll and dissipates that energy as heat (Erickson et al., 2015; Polle et al., 2000). This is a photoprotective mechanism and a major contributor to nonphotochemical quenching. These mechanisms are mostly short-term responses that the light-affected cells can use, however, if the cells are exposed to excess light levels for a long time, they make changes at the level of gene expression.

Another form of PSII non-photochemical response is the process of state transitions. This involves the reversible association of mobile LHCII with PSII (in state 1) and PSI (in state 2) (Goldschmidt-Clermont and Bassi, 2015). State transitions are believed to play a prominent role during the short-term by balancing the function of PSII and PSI and optimizing electron transport. State transitions are also thought to help balance the production of NADPH and ATP to ensure that the correct ratio of these two energy sources is available for carbon fixation. The State Transition 7 kinase (STT7 in *Chlamydomonas reinhardtii* or STN7 in higher plants) regulates the state transitions (Figure 1.6). Redox changes in the PQ pool activate the STT7 kinase activity (Berry et al., 2011; Goldschmidt-Clermont and Bassi, 2015). As the PQ pool becomes more reduced, limiting PSII activity, STT7 phosphorylates LHCII proteins. When phosphorylated, the LHCII proteins migrate away from PSII and transfer absorbed energy to PSI instead. If the PQ pool becomes more oxidized STT7 becomes less active, the corresponding phosphatase removes the phosphate from LHCII, and the antenna reattaches to PSII. State transitions are a prominent phenomenon in *C. reinhardtii*, where close to 80% of the light harvesting complexes can reversibly migrate between PSII and PSI following redox-driven phosphorylation.

Much less is known about the protection of PSI during light stress events. It is known that PSI can become damaged by excess light, but the process is more challenging to study and much slower than the PSII damage-repair cycle.

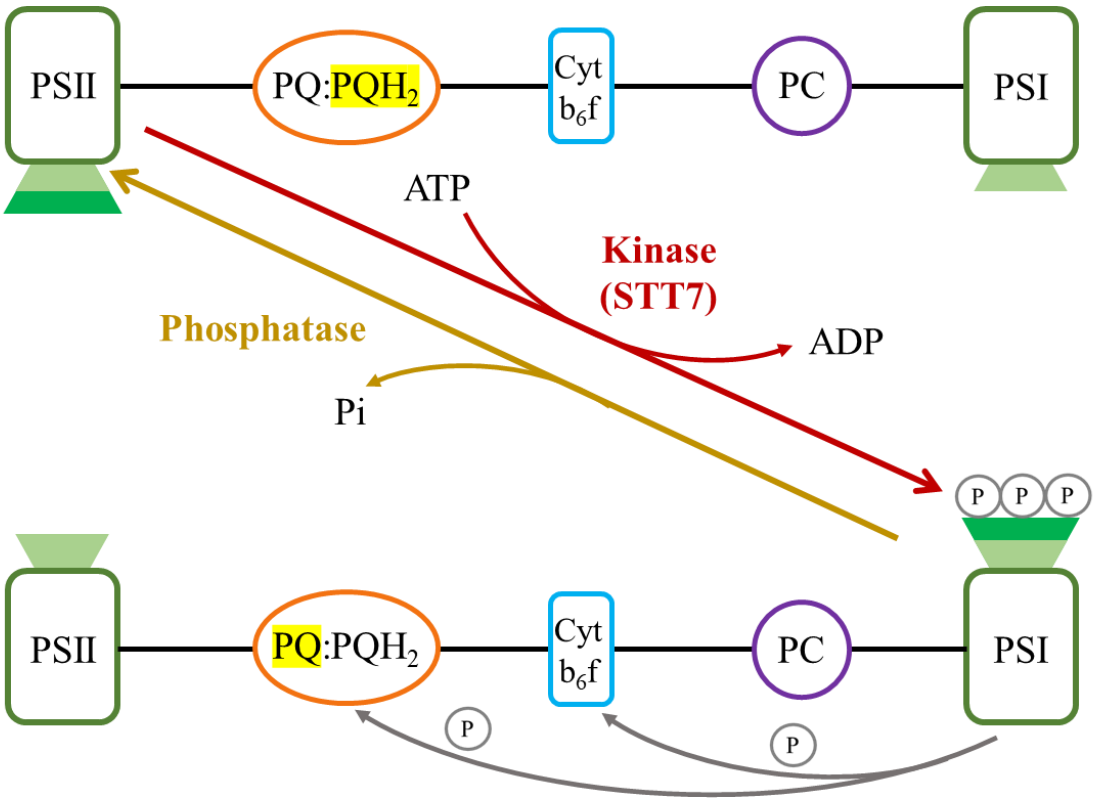

Figure 1.6. Schematic representation of state transitions in *C. reinhardtii*. Under conditions where the PQ:PQH_2 ratio favors the reduced state, the STT7 kinase is activated and it phosphorylates LHCII proteins. This leads to the migration of LHCII complexes to PSI where they increase PSI light harvesting capacity. In doing so, the electrons are drawn out of the electron transport chain more quickly than they enter, resetting the PQ:PQH_2 ratio favoring a more oxidized state. In turn, this decreases the activity of STT7 until a steady state is reached. This figure is redrawn based on work presented in (Goldschmidt-Clermont and Bassi, 2015).

1.4. The *psaF* mutant

In an attempt to study the role of the PSAF subunit of PSI, Farah et al. (1995) found that *psaF* cells exhibited decreased electron transfer from plastocyanin to PSI (Farah et al., 1995). It was discovered that while the cells could grow photoautotrophically and assemble a functional PSI, they could not tolerate exposure to high light (Farah et al., 1995; Hippler et al., 2000). While studying the *psaF* strain, Hippler et al. (2000) discovered a spontaneous suppressor mutation, that allowed the cells to survive at light intensities greater than 750 µmol photons m^{-2} s^{-1}, or High Light (HL) conditions. Examining the LHC protein complexes of the *psaF* suppressor, it was clear that the cells failed to properly insert the LHC proteins into the thylakoid membrane, thus they were non-functional (Hippler et al., 2000). The PSAF subunit is bound to the PSI reaction centre by protein-protein interactions and it is the site for docking plastocyanin. Unfortunately, Hippler lost the *psaF* suppressed strain before he could identify the mutation. However, this led to a hypothesis that nuclear encoded genes exist that are required for the proper insertion and alignment of LHC proteins in the thylakoid membrane.

The PSAF protein acts as a docking site for plastocyanin and aids in the transfer of electrons to PSI. When the *psaF* mutant was exposed to HL, PSI was excited at a rate that is greater than the rate at which it can be reduced by plastocyanin. This resulted in P700 staying in an excited state, with an increased possibility of charge recombination. While PSI is not thought to be a site of singlet oxygen production in the chloroplast, the *psaF* mutant is killed by oxidative reactions when exposed to high light. However, as Hippler demonstrated, when grown under anaerobic conditions the *psaF* strain could grow at light levels above 1000 µmol photons m^{-2} s^{-1} (Hippler et al., 2001).

To test the ability to grow under light stress and different media conditions, and identify LHC chaperone-like proteins, *psaF* cells were transformed using a paromomycin resistance cassette, allowed to grow for 7 days, then exposed to high light (>750 µmol photons m^{-2} s^{-1}). Colonies that survived were examined further. The first colony to have the insert mapped acted as a proof of concept (Berry et al., 2011). While it did not identify an LHC insertion defect, the mutation was mapped to *STT7* (Berry et al., 2011). It was suggested that the loss of LHCII migration protects PSI from excess light, allowing the cells to survive under high light conditions (Berry et al., 2011).

In the case of the *stt7* suppressor of *psaF*, the diminished capacity of PSI activity due to the *psaF* deletion resulted in a more reduced electron transport chain (Berry et al., 2011). Normally, as the electron transport chain becomes more reduced, the STT7 kinase is activated, phosphorylating LHCB proteins that then migrate to PSI (Goldschmidt-Clermont and Bassi, 2015). The result of this process is PSI absorbing even more light energy and increasing photodamage. Based on these findings, any mutation that allows *psaF* cells to survive high light exposure must be protecting PSI.

The explanation centred on the impact of the *psaF* mutation. The slow transfer of electrons into PSI from PC (Figure 1.6) would result in a more reduced PQ pool, due to feedback processes. The more reduced PQ pool would lead to STT7 activation and hence LHCII phosphorylation and migration to PSI. The result would be more light being absorbed by PSI. It was suggested that this type of donor-side limited PSI function leads to oxidative stress (Berry et al., 2011; Hippler et al., 2000; Rochaix, 2002). However, the mechanism to this was not clear. It was not expected to be due to singlet oxygen production, however, some donor site limited Chlamydomonas strains do accumulate high levels of lipid peroxides compared to wild type cells exposed to high light (Somers et al., 2003).

Based on these observations - that suppressor mutations of the *psaF* high-light lethal phenotype must protect PSI from over-excitation - other colonies to be investigated may also exhibit decreased LHC proteins attached to PSI. A second colony obtained in the suppressor screen exhibited a pale green phenotype, compared to wild type cells, and was labeled *lgp1* (*light green phenotype 1*) according to the standard *C. reinhardtii* gene naming protocol (Dutcher SK, 1998). The *lgp1 psaF* strain was not as pale as the *psaF Chl b* deficient strain or the *psaF* suppressors described previously (Hippler et al., 2000), thus it was expected to be a new LHC-PSI defect mutant. The *lgp1 psaF* mutant grows photoautotrophically at light levels >1000 μmol photons m^{-2} s^{-1}. Using PCR based techniques the plasmid insertion was found to be located in chromosome 5, just upstream from the *PSAD* promoter. This region is poorly characterized. There are several nearby predicted genes and an EST mapped to a region with no predicted gene model. The insert segregated with the pale phenotype following backcrosses to the wild type strain. Interestingly, the pale phenotype is accentuated when cultures are growing rapidly.

Understanding how the *lgp1* mutation suppresses the *psaF* high-light lethal phenotype is the focus of the work presented in my thesis.

1.5. Research goals and hypotheses

The overall objective of this research is to understand the mechanistic process behind the *lpg1* phenotype of the C73 cells. Based on its pale green phenotype, I expect that it will have a defect in light harvesting processes that supresses the *psaF* high-light lethal phenotype. I also expect that this work will also help explain how Light Harvesting Complexes proteins are inserted and arranged in the thylakoid membrane on individual living cells of *Chlamydomonas* spp. As proved by (Nellaepalli et al., 2018), essential proteins such as YCF3-Y3IP1 and YCF4 have been previously identified as chloroplast-encoded accessory factors that modulate the assembling of PSI RC and PSI-LHC, respectively.

It has been previously hypothesized that the improper insertion of the LHC proteins would protect *psaF* cells from high light exposure (Hippler et al., 2000), and that *psaF* cells could survive HL conditions when also having the *stt7* mutation (Berry et al., 2011). Therefore, because C73 cells had both the *psaF* and *lgp1* mutations, I could infer that the *lgp1* mutation affected the LHC accumulation, assemblage or function. To investigate further, the following hypotheses were identified:

1) The *light green phenotype 1* mutation protects *psaF* cells allowing their survival under high light. The *lgp1* cells are pale green, which suggests lower chlorophyll levels.
2) Based on previous observations by (Berry et al., 2011; Hippler et al., 2001), I hypothesized that the *lgp1* mutation alters the Light Harvesting Complexes function to decrease the delivery of light energy to Photosystem I.

CHAPTER 2

2. MATERIAL AND METHODS

2.1. Algae cultivation and growth conditions

The *Chlamydomonas reinhardtii* cell types used in this study are described below and presented in Table 2.1. CC-125, CC-4533 and CC-5155 were obtained from the Chlamydomonas Resource Center (University of Minnesota, St Paul, MN, USA) and constitute the wild type (WT, mt+) lines used as control for the experiments carried out in this study. CC-125 is mating type plus (*mt+*). CC-4533 and CC-5155 are cell wall deficient strains (*cw15*) chosen because they electroporate well and are better for DNA and RNA extraction. CC-1355 is a Chlorophyll b mutant (*cbn1-48*), it is mating type minus (*mt-*), and it was also obtained from the Chlamydomonas Resource Center. For this study, CC-1355 is used as a low LHC-accumulating control for investigations into the *lgp1* strain. The 3bf mutant line is a *psaF* deficient strain acquired courtesy of Dr. J-D Rochaix (University of Geneva, Geneva, Switzerland). It was generated through a mutagenic screen (Farah et al., 1995). It is a useful tool when studying the impact of high light on cells as it dies under light levels above 750 μmol photons m^{-2} s^{-1}, which are considered High-Light (HL) conditions (Allorent et al., 2013; Berry et al., 2011). The C73 strain was obtained from a mutagenic screen looking for suppressor mutations of *psaF*. It was selected under HL on minimal media. Thus, it has capacity for photoautrophic growth on minimal media under HL. Due to its pale green colour, it was denoted *light green phenotype 1* (*lgp1*). The C73 strain is *cw15 and* also missing the PSAF subunit of PSI (*psaF*) and is resistant to paromomycin ($Paro^R$) - the selectable marker used in performing the suppressor screen. This strain is mating type minus (*mt-*). The C1 strain is pale green (*lgp1*), cell wall deficient (*cw15*) and resistant to Paromomycin ($Paro^R$). It was obtained by crossing C73 with CC-5155 (Harris, 2008; Jiang and Stern, 2009). It allows the *lgp1* phenotype to be examined in the presence of a fully functional PSI where the PSAF subunit is present, and because it is *cw15* it can be more easily transformed with foreign DNA to rescue the *lgp1* phenotype.

Table 2.1. Description of the *C. reinhardtii* cell types used in this study with their individual genetic and phenotypical properties.

Strain	**Genetic properties**	**Phenotype**	**References**
CC-125	WT, *mt+*	Wild type, mating type +	(Pröschold et al., 2005)
CC-5155	*cw15 · mt+*	Cell wall deficient, mating type +	(Jonikas CMJ030 F5 backcross strain [E8])
CC-4533	*cw15 · mt-*	Cell wall deficient, mating type -	(Jonikas CMJ030)
CC-1355	*cbn1-48 · mt-*	Pale green	(Tanaka et al., 1998)
3bf	*psaF*	High Light sensitive	(Farah et al., 1995)
C73	*lgp1 · psaF · cw15 · mt-*	$Paro^R$, pale green/yellow	
C1	*lgp1 · cw15*	$Paro^R$, pale green/yellow	

C. reinhardtii cultures were maintained on solid Tris-Acetate-Phosphate medium (TAP - the chemical composition is supplied in Table 2.2) (Gorman and Levine, 1965; Harris, 2008) complemented with 2.5 mg L^{-1} arginine and 1.5% agar (Millipore-Sigma, Darmstadt, Germany). For performing the required experiments, strains were transferred to liquid TAP medium in sterile 250 mL Erlenmeyer flasks and grown under uniform light conditions of 100 µmol photons m^{-2} s^{-1}, for 4 days on a Thermo Scientific MaxQ 3000 orbital shaker at 125 rpm and 24°C.

2.2. Chlorophyll extraction and quantification

For chlorophyll extraction, cells were grown in liquid media to mid-log phase and a density of approximately 4-6 · 10^6 cells mL^{-1} (Harris, 2008). Cells were counted by fixing 30 µL of each culture with iodine and using an haemocytometer (Camacho-Fernández et al., 2018; Hanks and Wallace, 1958). Subsequently, 500 µL of cells were harvested by centrifugation at 2000 g for 5 minutes using an Eppendorf Centrifuge 5417C. The supernatant was discarded, and the remaining pellet was resuspended in 500 µL of 80% acetone: water (v/v). Subsequently, 35 mg of glass beads were added to the acetone mixture and cells were disrupted by two cycles of 20 seconds on High using a Mini-Beadbeater (Biospec Products). The mixture was then centrifuged at 5000 g for 5 minutes to remove cell debris, and the supernatant was transferred to semi-micro cuvettes (ThermoFisher 14-955-127). The absorbances at 647 nm and 664 nm were recorded with a Thermo Spectronic Genesys 20 spectrophotometer, which was zeroed at 750 nm to correct for any remaining debris. The total amount of chlorophyll along with the chlorophyll a to chlorophyll b ratio (Chl *a*/ Chl *b*) were calculated according to Porra and Scheer, 2019 and presented on a per cell basis (Table 2.3).

2.3. SDS PAGE and immunoblotting

Due to the considerable variation in chlorophyll levels on a per cell basis amongst the different samples, immunoblotting experiments were performed on an equal protein basis. However, chlorophyll extraction was needed in order to perform a Lowry's protein assay (Lichtenthaler and Buschmann, 2001; Peterson, 1977). For protein extraction, liquid cultures were grown for 4 days until the required cell density was achieved. Once the density was measured, 1 mL of fresh culture was transferred to an Eppendorf tube and centrifuged for 5 minutes at 2000 g. The supernatant was discarded, and the cell pellet was resuspended in 500 µL of Sample buffer (Table 2.4) and heated at 65°C for 5 minutes, followed by centrifugation for 10

Table 2.2. Chemical composition of Tris-Acetate-Phosphate (TAP) medium used for maintenance of *C. reinhardtii* cultures.

Stock Solution (SL)	**Volume**	**Component**	**Concentration in SL**	**Concentration in final medium**
Beijerinck salts (TAP salts)	25 mL	NH_4Cl	16 g L^{-1}	7.47 mM
		$MgSO_4 \cdot 7H_2O$	4 g L^{-1}	0.83 mM
		$CaCl_2 \cdot 2H_2O$	2 g L^{-1}	0.45 mM
1 M Phosphate solution $(K)PO_4$ pH 7	1 mL	K_2HPO_4 28.8 g in 100 mL	1.65 M	2.7 mM (in total)
		KH_2PO_4 14.4 g in 100 mL	1.05 M	
Hunter trace elements solution	1 mL	$Na_2EDTA \cdot 2H_2O$	0.5 g L^{-1}	134 µM
		$ZnSO_4 \cdot 7H_2O$	0.22 g L	136 µM
		H_3BO_3	0.114 g L^{-1}	184 µM
		$MnCl_2 \cdot 4H_2O$	0.05 g L^{-1}	40 µM
		$FeSO_4 \cdot 7H_2O$	0.05 g L^{-1}	32.9 µM
		$CoCl_2 \cdot 6H_2O$	0.016 g L^{-1}	12.3 µM
		$CuSO_4 \cdot 5H_2O$	0.016 g L^{-1}	10 µM
		$(NH_4)_6MoO_3$	0.011 g L^{-1}	4.44 µM
Tris base	2.42 g	$H_2NC(CH_2OH)_3$		20 mM
Acetic acid-glacial (titrated to pH 7.1–7.2)	≈ 1 mL	CH_3COOH		
Arginine	2.5 mg	L-(+)- Arginine JT Baker	2.5 mg L^{-1}	2.5 mg L^{-1}
Distilled Water	975 mL			

*Beijerinck salts and trace elements were prepared as stock solutions (SL) at the given concentrations beforehand and were added at the mentioned volumes to 1 L of final medium.

Table 2.3. Chlorophyll coefficients and equations used to quantify total amount of chlorophyll and Chl a to Chl b ratios.

Absorbances (nm)	**[Chl *a*]**	**[Chl *b*]**	**[Chl *a* + Chl *b*]**
	Extinction coefficients (Porra and Scheer, 2019)		
663.6 ($A^{663.6}$)	12.25	4.91	7.34
646.7 ($A^{646.7}$)	2.55	20.31	17.76

[Chl *a*] = $12.25 \cdot A^{663.6} - 2.55 \cdot A^{646.7}$ µg mL^{-1} ……..……(2.1)

[Chl *b*] = $20.31 \cdot A^{646.7} - 4.91 \cdot A^{663.6}$ µg mL^{-1} ……..(2.2)

[Chl *a* + Chl *b*] = $17.76 \cdot A^{646.7} + 7.34 \cdot A^{663.6}$ µg mL^{-1} ...……..(2.3)

Chl *a*/ Chl *b* = [Chl a]/ [Chl b]……...…….(2.4)

Table 2.4. Sample buffer required for protein extraction protocol.

Solution component	**Volume**	**Final concentration**
2X Lysis Buffer*	500 µL	1X
1M DTT	50 µL	50 mM
100X protease inhibitors (Sigma P9599)	10 µL	1X
200 mM NaF	50 µL	10 mM
H_2O	390 µL	

Sample buffer must be freshly prepared

Solution component for 2X Lysis Buffer*	**Volume**	**Final concentration**
0.5M Tris-HCl (pH 6.8)	2.5 mL	125 mM
Glycerol	2 mL	20%
10% SDS	4 mL	4%
H_2O	1.5 mL	

Lysis buffer can be prepared in stock and stored at RT

minutes at 12000 g and room temperature, and the supernatant was collected. The absorbance of the supernatant was measured at 647 nm and 664 nm, with the spectrophotometer zeroed at 750 nm, and the total chlorophyll concentration in each sample was calculated as by Porra and Scheer, 2019. Total protein was determined using the BioRad RC DC Protein Assay kit (ref. 500-0122), following the manufacturer's instructions. Samples were stored in equal 20 µg protein basis aliquots at -80°C when not used directly.

The SDS-PAGE protocol used 15% acrylamide/ bisacrylamide 37.5: 1 (v/v) gels prepared with 6 M urea following the instructions in the protocol by Fisher Scientific (catalog number BP169-500) (Król et al., 1999), and the protein ladder used was a PAGE-Ruler Plus Prestained Protein Ladder (Thermo Fisher, catalog number 26619). Samples were loaded onto the gels on an equal 20 µg protein basis per lane, alongside the ladder and the gels were run at RT using 50 Volts (V) for stacking and 100 V for resolving, until the dye front reached the bottom of the gel.

For immunoblotting, gels were transferred to polyvinylidene difluoride (PVDF) membranes using a wet transfer apparatus for 1 hour at 100 V and 4°C in transfer buffer (25 mM Tris, 192 mM glycine, 20% methanol, 0.01% SDS), and subsequently blocked for 1 hour at RT in 5% milk: TBST (v/v) (50 mM Tris pH 7.5, 150 mM NaCl, 0.1% Tween). Membranes were exposed to primary antibodies for 1 hour at RT except when exposed to Lhca3 and Lhca8 antibodies, which were blotted overnight at 4°C. Membranes were washed three times for 10 minutes in TBST at RT before incubation with secondary antibodies for 1 hour at RT. A full list of the antibodies used for immunoblotting and their dilutions is supplied in Table 2.5. All these procedures were carried out on a gel shaker. In order to enhance the chemiluminescence of the membranes, they were exposed to the Super Signal West Pico PLUS Chemiluminescence Substrate kit (Thermo Scientific, catalog number 34580) for 2 minutes at RT. Multiple exposures were recorded using a BioRad ChemiDoc MP digital imaging system. Densitometric analysis was performed using Image Lab software from BioRad. To compare loading and performance of the gels, an antibody recognizing the β subunit of the chloroplast ATP synthase enzyme complex was used, because it is relatively unaffected by growth conditions (Du et al., 2018; Oessner et al., 1986).

Table 2.5. Antibodies used to examine steady state protein levels.

Antibody	Host	Reference	Dilution
PSAA	rabbit	Agrisera AS06 172	1:5000
PSAD	rabbit	AS09 461	1:5000
PSBA	chicken	AS01-016	1:10000
PSBB	rabbit	AS04-038	1:5000
CYTF	rabbit	AS06 119	1:50000
ATPB	chicken	AS03-030	1:10000
LHCB2	rabbit	AS01-003	1:10000
LHCB4 (CP29)	rabbit	AS06-117	1:20000
LHCB5 (CP26)	rabbit	AS09-407	1:20000
LHCBM5	rabbit	AS09-408	1:20000
LHCA1	rabbit	(Bassi et al., 1992)	1:10000
LHCA2	rabbit	(Bassi et al., 1992)	1:10000
LHCA3	rabbit	(Bassi et al., 1992)	1:2000
LHCA4	rabbit	(Bassi et al., 1992)	1:4000
LHCA5	rabbit	(Bassi et al., 1992)	1:4000
LHCA6	rabbit	(Bassi et al., 1992)	1:10000
LHCA7	rabbit	(Bassi et al., 1992)	1:2000
LHCA8	rabbit	(Bassi et al., 1992)	1:2000
LHCA9	rabbit	(Bassi et al., 1992)	1:4000
Anti-chicken IgY, HRP conjugate		A9046; Sigma	1:10000
Anti-rabbit IgG, HRP conjugate		W4011; Promega	1:20000

2.4. 2D-Blue native polyacrylamide gel electrophoresis (BN-PAGE)

Immunoblotting from SDS-PAGE gives an indication of the relative abundance of a given protein. However, the LHC and photosystem proteins only function properly as parts of large complexes. To investigate the large thylakoid membrane protein complexes, blue-native PAGE was used (Järvi et al., 2011; Schägger and von Jagow, 1991). Membrane enriched fractions of *C. reinhardtii* cells were loaded onto gels on an equal 10 µg chlorophyll basis as the focus of this experiment was studying the photosynthetic machinery. For such purpose, each strain was grown in separate liquid TAP cultures for 4 days, as described in section 3.1, until the desired cell density was achieved. Cells were pelleted for 5 min at 2000 g andamples were further treated as per manufacturer's instructions in NativePAGE Novex Bis-Tris Gel System protocol (Thermo Fisher catalog number P-9599). Two Blue Native gels were run each time. NativePAGE 3-12% Bis-Tris gels (Thermo Fisher, catalog number BN2011BX10). with Native Mark unstained Protein Standards (Life Technologies, Thermo Fisher, catalog number LC0725). Each gel was run at 4°C with voltage intervals of 75 V for 30 minutes, 100 V for 30 minutes, 125 V for 30 minutes, 150 V for 1 hour and 175 V until the dye front reached the bottom of both gels.

The first BN gel obtained was used for Coomassie Blue analysis. The gel was microwaved for 45 seconds in 100 mL fix solution (40% methanol, 10% acetic acid) and placed on the gel shaker for 15 minutes at RT. Subsequently, the fix solution was discarded and replaced by 100 mL destain solution (8% acetic acid) and microwaved for 45 seconds. The gel was then shaken at RT until the required background was achieved. The second BN gel was used for running the 2D-PAGE. Individual lanes were cut from the gel and incubated in solubilization buffer (62.5 mM Tris-HCl pH 6.8, 10% glycerol, 2% SDS, 50 mM DTT) for 1 hour at RT with gentle agitation. The gel strips were transferred to the top of 15% SDS/Urea (v/v) gels, prepared as described previously (section 0), and sealed into place with 0.5% agarose in SDS-PAGE running buffer (25 mM Tris, 192 mM glycine, 0.1 SDS). Gel electrophoresis was run at 50 V through the stacking gel and at 100 V through the resolving gel, until the samples reached the bottom of the gel. The SDS-PAGE gels were transferred to PVDF membranes submerged in transfer buffer (25 mM Tris, 192 mM glycine, 20% methanol, 0.01% SDS) at 100 V for 1 hour at 4°C. In order to enhance the chemiluminescence of the membranes, they were exposed to Super Signal West Pico PLUS Chemiluminescence Substrate kit (Thermo Scientific, catalog number

34580) for 2 minutes at RT. All these procedures were carried out on a gel shaker. Multiple exposures were recorded using a BioRad ChemiDoc MP digital imaging system. A densitometric analysis was performed on immunoblot data using Image Lab software from BioRad.

2.5. 77K chlorophyll fluorescence spectroscopy

Algal samples were diluted to an equal chlorophyll concentration of 25 µg mL^{-1} and kept in the dark for 15 minutes before measuring. In an Eppendorf tube, 500 µL of culture was added to 500 µL of 50% glycerol: TAP (v/v) and mixed. The solution was transferred to ThermoFisher 5 mm 7-inch Bel-Art glass tubes (ref. 16-800-178) and quickly frozen in liquid nitrogen. The frozen samples were placed in liquid nitrogen held in a vacuum quartz dewer in a Horiba Fluoromax Steady State Spectrofluorometer (FLMAX-4C-L_1692D-1118-FM, Horiba, Japan). The front entrance and exit slits were both set to 5 nm bandpass. The excitation wavelength was 436 nm and the emission spectra were recorded from 660 nm to 800 nm, in 1 nm increments. The fluorescence emission spectra results were normalized to 682 nm wavelength and deconvoluted using OriginLab 2017 Graphing Software (64-bit/ b9.4.0.220 Academic version).

2.6. Cloning of the LGP1 area of interest

2.6.1. Bacterial artificial chromosome (BAC) isolation

The insert site of the *lgp1* mutation was determined using RESDA-PCR as described previously by (Berry et al., 2011; González-Ballester et al., 2005). This technique located a plasmid insertion upstream of the *PSAD* promoter on Chromosome 5, in a poorly characterized region of the *C. reinhardtii* genome. A BAC containing a copy of this genomic region was identified from the Chlamydomonas genome project and obtained from CUGI (Clemson University Genomics Institute) as an agar stab of *E. coli* cells. To obtain a purified BAC preparation, cells were streaked on solidified Luria Broth (LB) agar (1% w/v) plates supplemented with 12.5 µg mL^{-1} Chloramphenicol (Sigma Aldrich ref. C-1863) and grown at 37°C overnight. Colonies were kept on the LB plates at 4°C for future use. For the purpose of isolating small amounts of the BAC, single colonies were isolated from the LB plates and grown in 5 mL liquid LB plus 12.5 µg mL^{-1} chloramphenicol overnight at 37°C. DNA was extracted from these cultures using the *Isolation of BAC DNA from Small-scale Cultures* protocol as described in *Molecular Cloning: A Laboratory Manual* (Sambrook and Russell, 2001). When

larger amounts of the BAC were needed, the Isolation of BAC DNA Large-scale cultures protocol from *Isolation of BAC DNA from Large-scale cultures, Molecular Cloning: A Laboratory Manual* (Sambrook and Russell, 2001) was followed. DNA quality and integrity were measured using the Nanodrop 2000 Spectrophotometer (ThermoFisher ref. UZ-83061-12) and aliquots were examined by gel electrophoresis [EtBr, 1% agarose (EMD Chemicals)].

2.6.2. PCR and sequencing

All polymerase chain reactions (PCR) were performed using BAC DNA as a template for the Q5 High Fidelity Polymerase (New England Biolabs, MA, USA). The deoxynucleotide triphosphate PCR grade mix (10 mM) was acquired from Invitrogen (ThermoScientific, CA, USA). Primers were obtained from Invitrogen (ThermoScientific, CA, USA). A list of all the primers and their sequences is provided in Table 2.6. PCR were performed using an iCycler thermal cycler (Bio-Rad) using the following cycling conditions: initial denaturation at 98°C for 30 seconds, 38 cycles of 98°C for 10 seconds, 62°C for 30 seconds, cycling extension at 72°C for 30 seconds, and a final extension at 72°C for 2 minutes (Mackinder et al., 2017). Gel electrophoresis (EtBr, 1% agarose) was performed to confirm the products of the PCR products. Purification of DNA fragments from agarose gel was performed using Gel and PCR Extraction System (ref. 9K-006-0007-100) (BioBasic Inc., Markham, ON, Canada). Total concentration of DNA was measured using a Nanodrop 2000 Spectrophotometer (ThermoFisher). The amplified fragments and their hypothesised genomic regions are shown in Figure 2.1. PCR ampliconswere verified by sequencing (Eurofins, Toronto, ON, Canada).

2.6.3. Plasmid clones

The plasmid pLM006 (Mackinder et al., 2017) is designed to express a gene of interest tagged to an mCherry-His tag, driven by the *PSAD* promoter. It uses a hygromycin resistance cassette as a *C. reinhardtii* selectable marker (Mackinder et al., 2016). Hygromycin was chosen as a selectable marker because the C73 strain is already resistant to paromomycin. The complete map of pLM006 is supplied as Figure 2.2. Using the fragment amplified I do not expect to express a LGP1 mCherry fusion, but designed the oligonucleotides such that the first ATG belonging to a possible open reading frame up stream of the C73 insert site would be cloned under direct control of the pLM006 expression system of the *PSAD* promoter.

Table 2.6. Primer sequences designed for PCR-based amplification of the LGP1 region of the *C. reinhardtii* genome.

Name	**Sequence 5’ to 3’**
KW 326	GCTACTCACAACAAGCCCAGTTATGTGGCGTCGGCTG
KW 346	GAGCCACCCAGATCTCCGTTGAAACGGCGACTGAGCAGGAG
KW 82	ATGCGGCATATCTGTACTCCT
KW 353	CATGTGATTTGCCTACCCTCAACACC
KW 331	GAGCCACCCAGATCTCCGTT
KW 354	CCAGCAATTCCGACGACCCTAAATGC
KW 295	GGATGGTGACGATGAGCTGG
KW 344	GAGCCACCCAGATCTCCGTTCACCGTGGTTGCCGTCACTGAGC
KW 345	GAGCCACCCAGATCTCCGTTGAGCCAGCAATTCCGACGACC

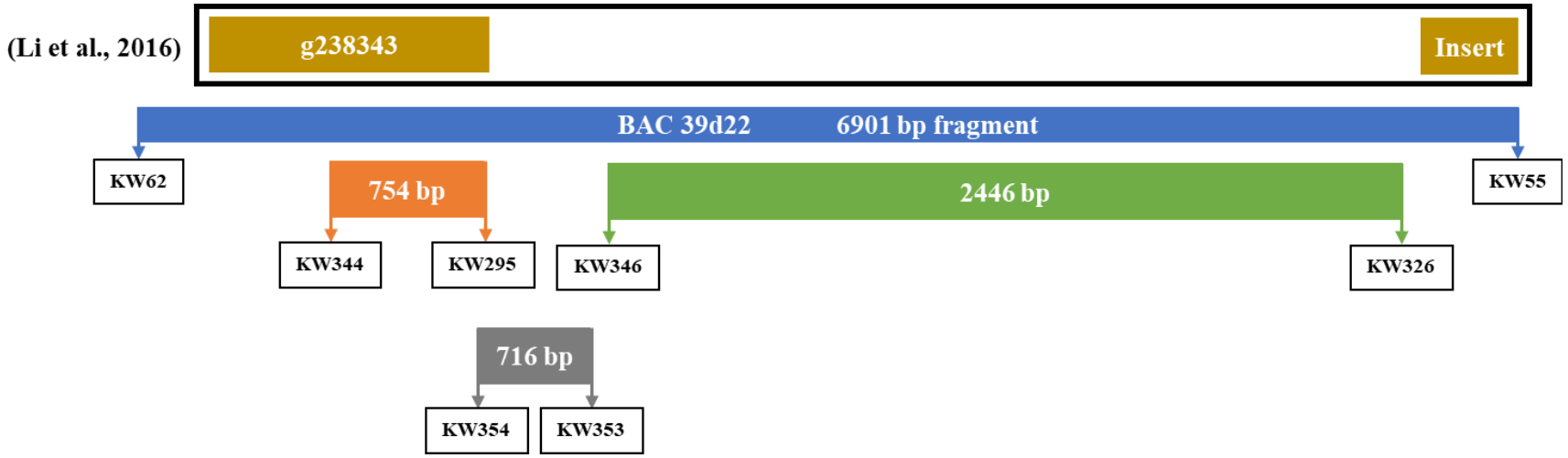

Figure 2.1. Map of the region of the *C. reinhardtii* genome suspected to encode the *LGP1* gene. Locations where oligonucleotides anneal for PCR are indicated. It was not possible to amplify the entire fragment in a single PCR therefore three overlapping fragments were synthesized and assembled. The location of the *PSAD* promoter plasmid insert is shown on the right, and the location of the nearest predicted gene model is shown on the left. The sequence used for this analysis was obtained from the *Chlamydomonas reinhardtii* v5.5 build (https://phytozome.jgi.doe.gov).

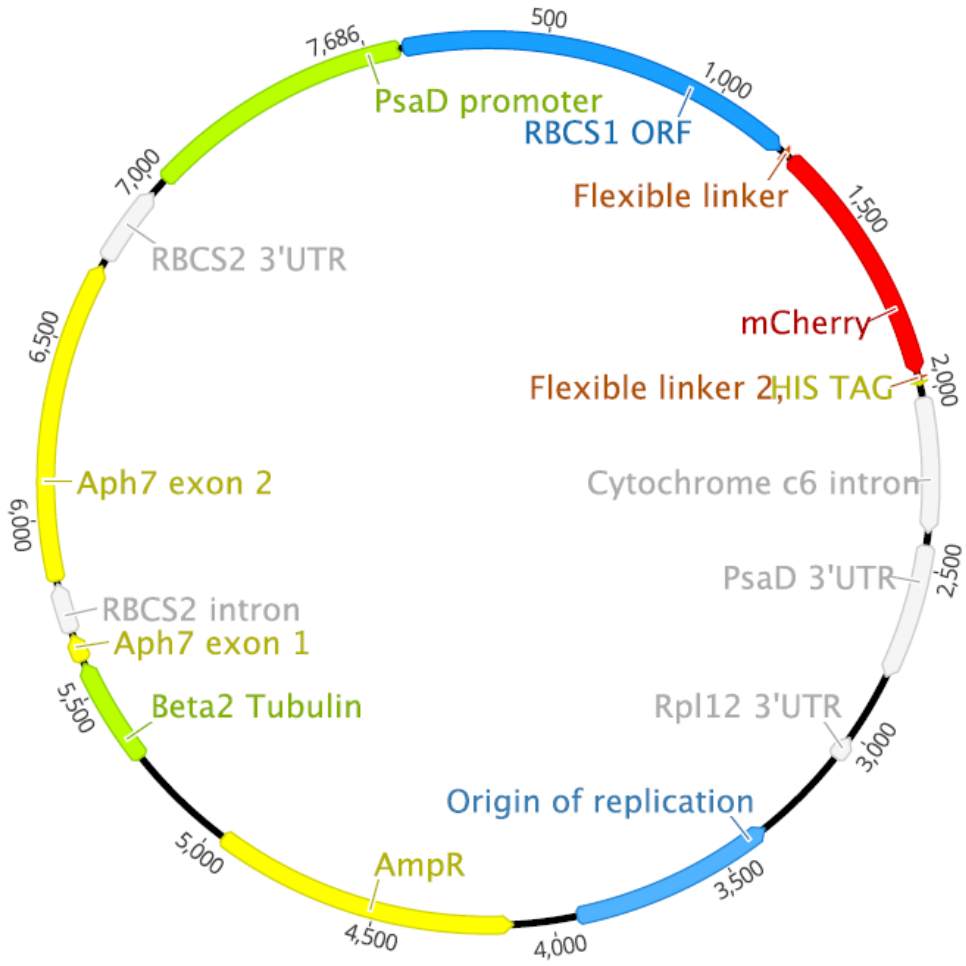

Figure 2.2. Map of pLM006 (Mackinder et al., 2017). The hygromycin^{R} gene and the KspAI site are referred as Aph7 and RBCS1 ORF, respectively.

E. coli cells containing the pLM006 plasmid were acquired from the Chlamydomonas Resource Centre (University of Minnesota, St Paul, MN, USA) and grown in solidified LB 1% agar (w/v) plates supplemented with 50 µg mL^{-1} ampicillin (IBI Shelton Scientific ref. IB02040) at 37°C overnight. After being streaked to single colonies, isolated colonies were selected for growth in 5 mL of LB liquid supplemented with 50 µg mL^{-1} ampicillin. Tubes were incubated at 37°C with shaking overnight. Plasmid DNA was extracted following *Molecular Cloning: A Laboratory Manual* (Green et al., 2012; Sambrook and Russell, 2001). Total DNA concentration was measured by spectrophotometry and confirmed by gel electrophoresis (EtBr, 1% agarose). The isolated pLM006 plasmid was digested with KspAI (ThermoFisher ref. ER1031) following the manufacturer's protocol and incubated at 37°C for 3 hours. The resulting fragments were analyzed by gel electrophoresis (EtBr, 1% agarose) and the longest fragment, which was about 6500 bp, was excised and cleaned from the gel using BioBasic Gel and PCR Extraction System. DNA integrity and concentration were measured using a spectrophotometer and confirmed by gel electrophoresis (EtBr, 1% agarose). For subsequent experiments, DNA concentration was calculated as follows:

DNA concentration = (mass in ng) x 1000 / (base pairs x 650 daltons) ……. (2.5)

To assemble the three PCR fragments into the digested pLM006 vector using NEBuilder HiFi DNA Assembly Cloning Kit (ref. E5520S), the manufacturer recommends between 0.2–0.5 pmols of each DNA fragment. This system partially digests double stranded DNA fragments by digesting 5' ends. This allows overlapping 3' ends to base pair, creating a single fragment. Nicks left behind are ligated to form a new version of the pLM006 plasmid that contains the suggested *LGP1* gene. This new plasmid was named pCM010. To perform the assembly reaction, the fragments were incubated in the master mix at 50°C for 60 min. For further experiments, the cloned plasmids were stored at -20°C.

2.6.4. Chemical transformation of high-efficient competent *E. coli* cells

The pCM010 plasmid was used for chemically transforming High Efficiency NEB 5-α Competent *E. coli* (ref. C2987I). These cells are DH5-α, T1 phage resistant and endA deficient specifically designed for high-quality plasmid preparations. In order to chemically transform the cloned plasmids with the DH5-α cells, the cells were first thawed on ice. When no crystals were observed, 2 µL of the cold assembly product were added to the competent cells. The content in

each tube was mixed by gently pipetting and placed on ice for 30 minutes. Subsequently, the mix was heat shocked at 42°C for 30 seconds and transferred to ice for 2 minutes. No vortexing or mixing was done in these two steps. Thereafter, 950 µL of supplied NEB SOC medium, stored at room temperature (RT), was added to each tube. All tubes were incubated at 37°C for 60 minutes while shaking at 2000 rpm. The bacterial selectable marker in pLM006 is ampicillin resistance, thus LB plates containing ampicillin (50 µg mL^{-1}) were warmed at 37°C. When the incubation process was completed, 100 µL of the transformed product was spread onto the selection plates and incubated overnight at 37°C. The viability of the transformed products was observed after 16 hours and plates with colonies were placed at 4°C until needed. To identify colonies containing the desired fragments, *E. coli* colonies were tested by colony PCR using oligos KW 295 and KW 331 (Table 2.6). For the presence of a 1000 bp fragment from pCM010 containing cells, five positive colonies were obtained from 50 colonies tested. The above described process was used to isolate the plasmid from the positive colonies and the DNA was sent for sequencing using pLM006 Forward (KW 295) and pLM006 Reverse (KW 331) oligos to Eurofins. Plasmids shown to contain the desired fragments (pCM010) were used to transform C1 and CC-4355 strains (Table 2.1) to determine if the cloned fragment could rescue the *lgp1* phenotype and restore wildtype chlorophyll levels.

CHAPTER 3

3. RESULTS

3.1. Differences in the phenotypic traits among *C. reinhardtii* strains

The C73 strain is paler green in colour than wild type *C. reinhardtii* cells but maintains capacity for photoautrophic growth on minimal media under high light, despite the presence of the *psaF* mutation. To confirm this aspect of its physiology, I compared its ability to grow on different growth media and under different light conditions. Solid Tris-Acetate-Phosphate (TAP) contains acetate as a reduced carbon source for algal growth and Tris-minimal media has no supply of reduced carbon (Gorman and Levine, 1965; Harris, 2008), were used as the growth media (Table 2.2). Cells were also exposed to three light conditions: High Light conditions (HL) ≈ 750 μmol photons m^{-2} s^{-1}, Growth Light conditions (GL) ≈ 70 μmol photons m^{-2} s^{-1}, and Dark conditions ≈ 0 μmol photons m^{-2} s^{-1}. The strains used in this experiment were CC-125, 3bF, CC-1355, C73 and *lgp1*-C1 (Table 2.1). When exposed to light levels ≈ 750 μmol photons m^{-2} s^{-1}(HL), the CC-125, CC-1335, C73 and *lgp1*-C1 strains survived on both media types (Figure 3.1, top panels). The C73 and *lgp1*-C1 strains exhibited a lighter green phenotype compared to CC-125 cells, when grown on Tris-minimal agar plates (Figure 3.1, top-right panel). Under HL conditions, the *psaF* deficient mutant line (3bF) died on both TAP and Tris-minimal media, as expected (Figure 3.1, top panels). Under GL conditions all strains grew normally on TAP medium, with a slightly less-green colour noticeable for the C73 and the *lgp1*-C1 colonies (Figure 3.1, middle-left panel). Similarly, the CC-1335 cells were paler green, as expected for a Chl b deficient strain (Figure 3.1, middle left panel). On Tris-minimal growth media, all strains grew more slowly, and they were paler in colour (Figure 3.1, middle-right panel). Lastly, under Dark conditions every strain displayed a yellow-in-the-dark phenotype when grown on TAP media (Figure 3.1, bottom-left panel). This is common in *C. reinhardtii* because the light independent *Proto-Chlorophyllide Oxidoreductase* (*DPOR*) gene seems highly susceptible to mutations (Gumpel et al., 1995).

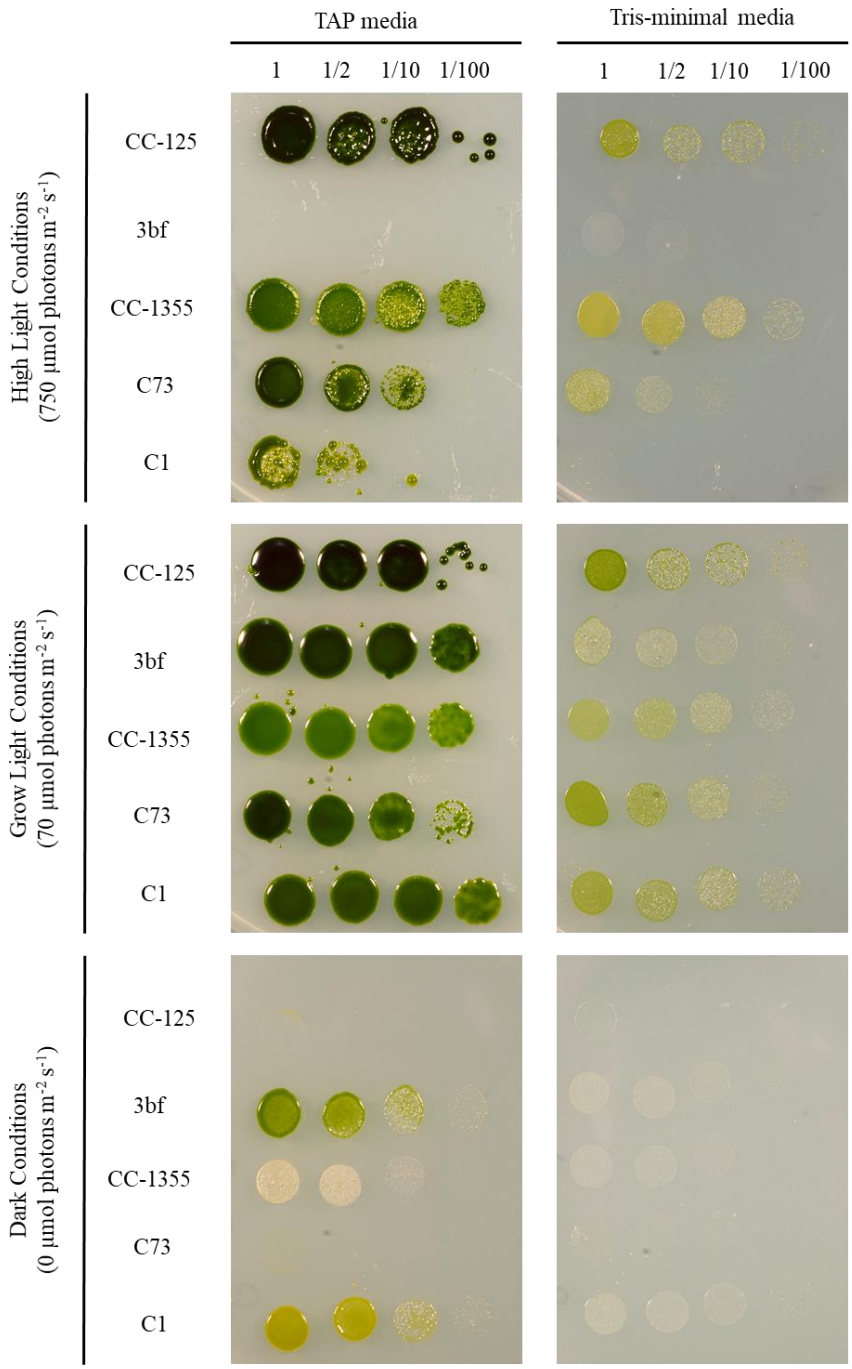

Figure 3.1. Culture growth limitations based on light and carbon source availability. Growth efficiency was examined by spotting 8 µL of culture normalized by Chl conc onto each plate's surface prior to exposure to high-light, growth-light or dark conditions. The CC-125 strain was the WT control, 3bf was the *psaF* mutant, CC-1355 was the chlorophyll b deficient mutant, C73 was the light-green phenotype mutant and C1 the offspring generated after backcrossing C73 with CC-4533 to remove the *psaF* mutation (Table 2.1).

The yellow in the dark phenotype makes the comparison of dark grown strains challenging, yet it should have no overall impact on cell light-sensitivity. None of the strains grew on Tris-minimal media in the dark (Figure 3.1, bottom-right panel). This was expected because they would have no source of reduced carbon.

3.2. Variation in cellular chlorophyll accumulation

The light-green phenotype observed in C73 and *lgp1*-C1 suggests that there is a diminished amount of chlorophyll when compared to the darker green CC-125 strain (Figure 3.1, middle-left panel). Chlorophyll content of CC-1355 was measured in addition to the pale green mutant lines (C73 and *lgp1*-C1) and a cell wall deficient WT strain (CC-4533) (Table 2.1). CC-1355 contains a mutation in the *Chlorophyll a Oxidase* gene *cbn1-48* causing a chlorophyll b-less phenotype, which will result in low Chl b concentrations and a high Chl a to b ratio. To investigate this qualitative observation, I measured chlorophyll levels in the different strains of interest. Cultures were grown in TAP medium under GL conditions (70 µmol photons m^{-2} s^{-1}). WT cells contained 789 fg Chl a/ cell (Table 3.1), which was 12.7% higher than the C73 pale phenotype mutant cells with 689 fg Chl a/ cell (Table 3.1). However, the C73 and *lgp1*-C1 cells showed higher Chl a/ Chl b ratios, 2.15 and 2.46 respectively suggesting a decrease in LHC protein accumulation relative to the amount of the reaction centres (Table 3.1). The CC-1355 strain was included as a control. It lacks the *Chlorophyll a Oxidase* gene and thus accumulates very low levels of Chl b. While it contained 885 fg Chl a/ cell (Table 3.1), it had a very high Chl a/ Chl b ratio of 19.2 (Table 3.1). Thus, *lgp1*and C1 are notchlorophyll b deficient strains.

3.3. Photosystem stoichiometry

A reduction in cellular chlorophyll could reflect an overall decrease in photosynthetic components, a decrease in photosystem abundance, or a decrease in light harvesting proteins. To investigate which of these possibilities may be occurring in C73 cells, I performed semi-quantitative immunoblots (Figure 3.2, Figure 3.3, Figure 3.4, Figure 3.5). I selected protein components of the major thylakoid membrane complexes (Figure 3.3): PSAA and PSAD for photosystem I, PSBA and PSBB for photosystem II, PETA for the cytochrome b_6/f complex, and ATPB for the ATP synthase. Aliquots of thylakoid membrane enriched fractions from each strain were loaded onto a SDS-PAGE system on an equal protein basis, as described in section 2.3.

Table 3.1. Chlorophyll quantification and correlation between the *C. reinhardtii* strains of interest. Liquid cultures were grown in TAP media conditions, until a mid-log phase and a density of approximately 4-6 · 10^6 cells mL^{-1} was reached. The values shown are fg of chlorophyll per milliliter of culture. Calculations expressed per cell basis. These calculations are based on 15 different measurements (n=15) ± standard deviation.

Strains	**Chl *a*** **(fg/ cell)**	**Chl *b*** **(fg/ cell)**	**Chl *a* + Chl *b*** **(fg/ cell)**	**Chl a/b**
CC-4533	789±0.07	417±0.05	1206	1.89±0.02
CC-1355	885±0.62	46.1±0.05	931.1	19.2±1.37
C73	689±1.07	321±0.53	1010	2.15±0.03
C1	728±0.86	296±0.36	1024	2.46±0.02

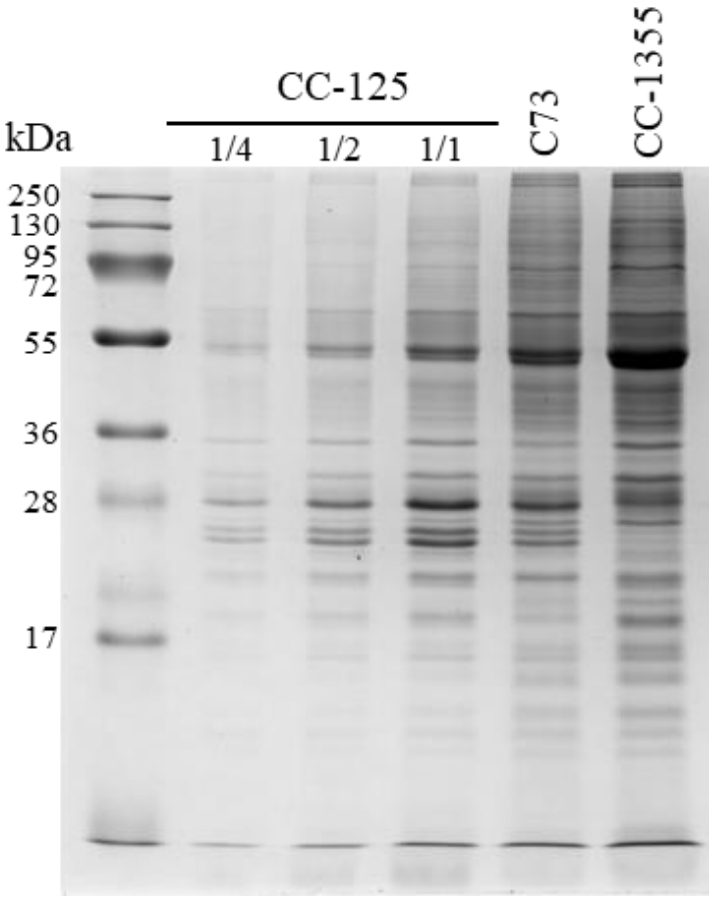

Figure 3.2. SDS-PAGE gel (Coomassie Blue stained) of the strains of interest. The gel shown above demonstrates the loading and resolution obtained using the system described in 2.3. CC-125 was used as control and the crude differences in LHC protein abundance (22-36 kDa range) were observed. The gel shown is representative of 5 repeats using cells from different batch cultures.

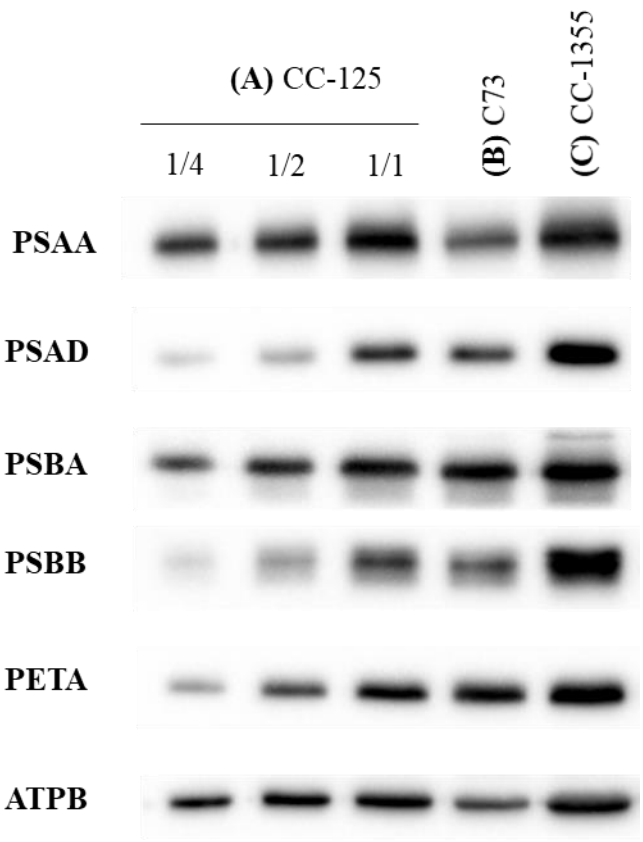

Figure 3.3. Comparative relative stoichiometry study performed in isolated thylakoid membranes having the same protein basis aliquots. In this study, CC-125 constitutes the Wild Type, C73 is our mutant strain of interest, and CC-1355, is a chlorophyll b deficient mutant (Table 2.1). Six photosynthetic subunits were analyzed: **PSAA** and **PSAD** belong to Photosystem I, **PSBA** and **PSBB** to Photosystem II, **PETA** is part of the Cytochrome b_6 f complex and **ATPB** is a component of the chloroplast ATP synthase, used in this experiment as a loading control. The blots shown above are representative of 5 repeats using cells from different batch cultures.

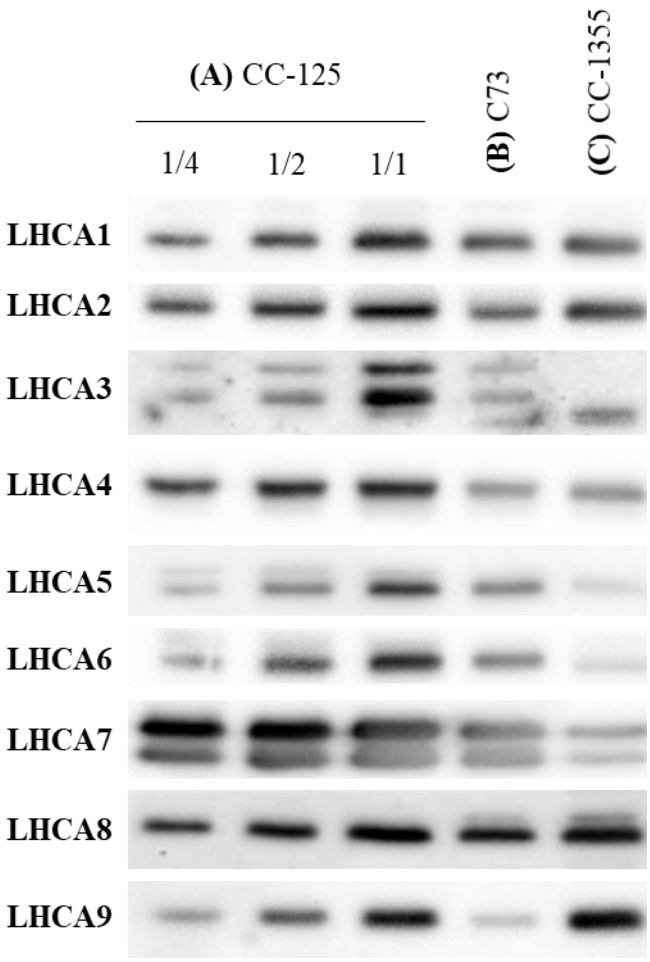

Figure 3.4. Immunoblotting study exposing the strains of interest to *LHCA* antibodies. Isolated thylakoid membrane samples were loaded on an equal protein basis to compare the relative abundance of nine different Light Harvesting Complex I proteins present in *C. reinhardtii*. CC-125 is the Wild Type, C73 is the mutant strain of interest, and CC-1355, is a Chlorophyll b deficient mutant (Table 2.1). The blots shown above are representative of 5 repeats using cells from different batch cultures.

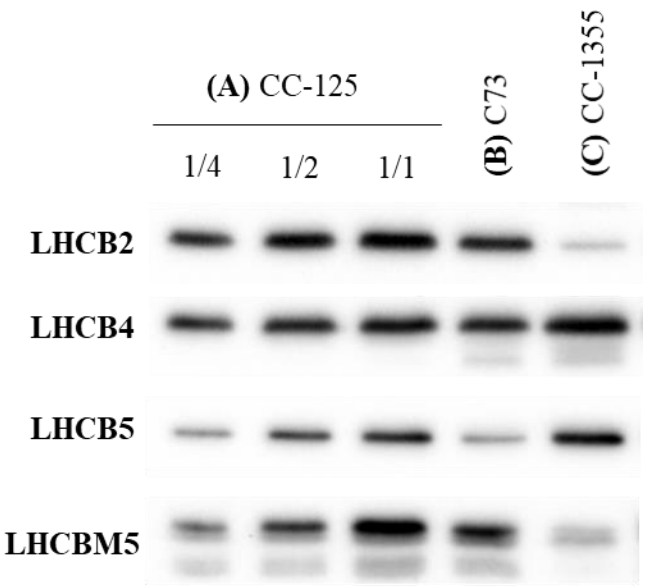

Figure 3.5. Immunoblotting study of isolated thylakoid membranes comparing the relative abundance of four different Light Harvesting Complexes proteins present in Photosystem II. CC-125 constitutes the Wild Type, C73 is the mutant strain of interest, and CC-1355 constitutes the Chlorophyll b deficient mutant (Table 2.1). The blots shown above are representative of 5 repeats using cells from different batch cultures.

The C73 strain accumulated lower levels of photosystem I, photosystem II, and the ATP synthase on a per membrane protein basis when compared to the WT cells (Figure 3.3). In the membranes of C73 cells, PSAD, PSBA and PSBB subunits accumulated at about 75% of the level observed in WT cells. The ATPB protein accumulated to approximately 50% of the amount observed in WT cells (Figure 3.3). The amount of PSAA protein accumulated to only about 25% of CC-125 levels. However, the amount of PETA is approximately the same in C73 as in CC-125 cells (Figure 3.3). In comparison, the CC-1355 cells had higher amounts of each complex when compared to CC-125. This is not surprising because CC-1355 accumulates low levels of most of the LHC proteins and thus, the photosystems, cytochrome b_6/f complex, and ATP synthase will constitute a greater percentage of the total protein in the thylakoid membrane. Looking at the overall stoichiometric differences in photosystem abundance in the three strains, it appears that C73 cells have a reduced level of PSI with respect to PSII and the Cytochrome b_6/f complex.

3.4. Light Harvesting Complexes (LHC) subunit abundance

Following the examination of photosystem stoichiometry, I wanted to determine if there were significant changes in the accumulation of LHC proteins in the C73 mutant. Based on the work of Hippler et al., (2000) and Berry et al., (2011) diminished LHC abundance would help account for the suppression of the *psaF* high-light-lethal phenotype observed in the C73 strain. Using available antibodies for four different LHCB proteins (LHCB2, LHCB4, LHCB5, and LHCBm5) and nine LHCA proteins (LHCA1-9), I examined their relative abundance in C73 compared to CC-125 and CC-1355 strains (Table 2.1). Because LHCB and LHCA proteins are organized separately, I studied the LHCA proteins first (Figure 3.4). In the case of the LHCA proteins, all except LHCA8 showed diminished accumulation in C73 cells compared to the CC-125 cells, usually in the 25 to 50% range except LHCA9, which accumulated in the >25% range (Figure 3.4). In their overall accumulation, C73 cells contain a greater abundance of LHCA proteins compared to the Chl b deficient strain CC-1355. However, LHCA1, 2, 4, and 8 accumulate to similar levels in CC-1335 as that observed in C73 cells (Figure 3.4). This correlates with the cellular chlorophyll abundance and the chlorophyll a to b ratio (Table 3.1).

We have a more limited range of LHCB antibodies available for *C. reinhardtii*. While it is predicted, based on the *C. reinhardtii* genome annotation, that there are also nine different LHCB genes (Natali and Croce, 2015), we only have access to four LHCB specific antibodies.

LHCB4 and LHCB5 correspond to minor antenna proteins of higher plants, while LHCB2 and LHCBM5 are part of the major light harvesting complex. The difference observed in LHCB accumulation was not as great as that observed for the LHCA proteins (Figure 3.5). LHCB2 and 4 accumulated to about 75% of the CC-125 levels. However, the abundance of LHCB5 and LHCBM5 were much lower in the C73 strain, accumulating in the 25% and 50% range, respectively. The chlorophyll b deficient mutant, CC-1355, did show significant lower levels of LHCB2 and LHCBM5, both accumulating to less than 25% of the amount observed in CC-125 (Figure 3.5). However, LHCB4 and LHCB5 accumulated at slightly higher levels than CC-125, and significantly higher levels than C73. These results indicate that C73 accumulates lower amounts of some LHCA and LHCB proteins, but not to the level observed in the chlorophyll b deficient mutant.

3.5. Blue Native (BN) gel electrophoresis

The data I obtained relating to the accumulation of chlorophyll and LHC proteins in C73 suggested smaller light harvesting antennae in the C73 strain. However, it seems that the reduction in LHC content is related to specific subunits, rather than a uniform decrease in all components (Figure 3.4 and Figure 3.5). Thus, the functionality of the antennae in C73 may be quite different than that of CC-125 or CC-1355. BN-PAGE was used to better understand how the diminished LHC content impacts the overall arrangement of LHC proteins in the thylakoid membrane and the attachment of the LHC proteins to the reaction centres(Figure 3.6). This technique resolves large protein complexes by molecular weight, while maintaining their native arrangement. The samples were loaded on an equal chlorophyll basis utilizing an equal chlorophyll: detergent (v:v) ratio. I compared the three different strains to show the potential differences I thought could explain the *lgp1* phenotype. The CC-125 strain was the wild type control, while CC-1355 had more significantly reduced accumulation of LHC proteins (Figure 3.4 and Figure 3.5). C73 LHC organization was compared to the normal (CC-125) and minimal (CC-1355) expectations. The proteins of both PSII-LHCII and PSI-LHCI super-complexes (Aro, 2004) showed significant lower intensity in both C73 and CC-1355 compared to the wild type strain. On the other hand,both C73 and CC1355 had much higher amounts of the PSII monomer than CC-125. A similar observation was made for the PSI-LHCI super-complexes (Figure 3.6).

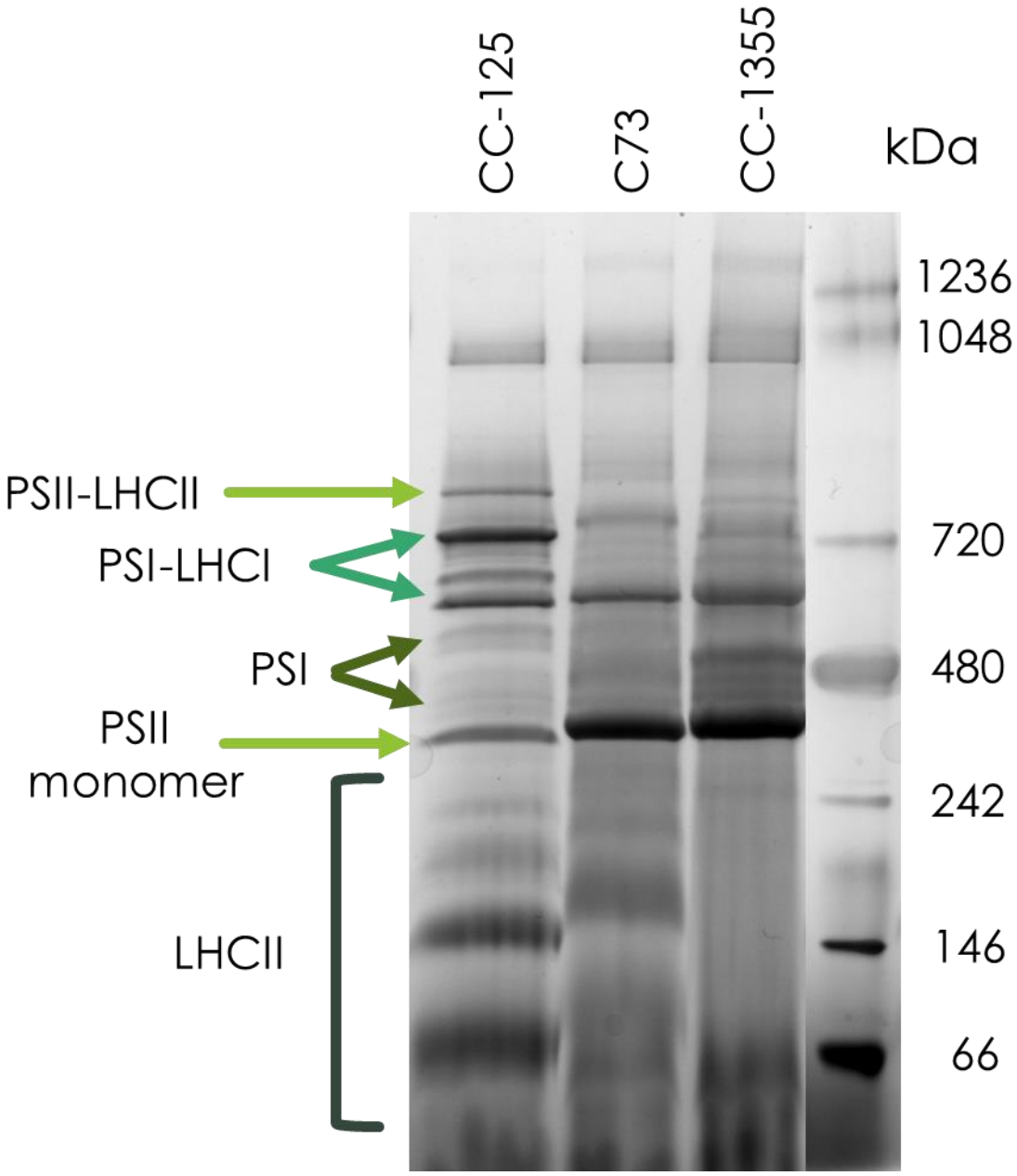

Figure 3.6. Blue Native gel electrophoresis of CC-125 as wild type, C73 as the mutant of interest and CC-1355 as the chlorophyll b deficient strain (Table 2.1). The figure shows the different protein super complexes separated according to their molecular weight and their functionality in the strains studied. The gel shown above is representative of 3 repeats using cells from different batch cultures.

The amount of the larger complexes observed in CC-125 was much greater than in C73 or CC-1355. These data suggest that C73 is unable to assemble or stabilize Photosystem Reaction Centre-LHC complexes.

To confirm the RC-LHC defect, 2D immunoblotting was performed on C73 and CC-125. The first dimension used BN-PAGE, followed by SDS-PAGE in the second dimension. The 2D immunoblot of CC-125 cell samples, using antibodies raised against the PSAA protein, identifies the presence the PSAA protein at about 60 kDa (Figure 3.7). At the top-left corner of the BN-PAGE gel, protein spots indicate the presence of very large PSI complexes (Figure 3.7, blue solid square). Moving to the right of the blot, dots can be observed that fall within the expected size range for PSI-LHCI and PSI complexes (Figure 3.7, green solid rectangle). When comparing to the C73 immunoblot, the very large complexes are not observed (Figure 3.7 middle-bottom image). There are, however, smaller above PSI-LHCI, and PSI complexes (Figure 3.7, green dashed rectangle). The effects of the C73 mutation can similarly be observed using antibodies raised against LHCA1 (Figure 3.8). In CC-125 cells, there are spots representing very-large PSI-LHCI complexes that did not solubilize well in the second dimension (middle-right, yellow rectangle), and bands at 20-40 kDa that represent PSI-LHCI and LHC complexes (Figure 3.8, bottom-middle image, red rectangle). There is also a strong spot at about 32 kDa that is located at the top range of LHC proteins in the BN-PAGE dimension, but it is not clear what this signal represents (Figure 3.8, blue dotted line). When examining the C73 sample, again the very large PSI-LHCI complexes are not detected and the signal at 20 kDa, which represents LHCA1 is more evenly spread through the BN-PAGE dimension (Figure 3.8, bottom image, red dashed rectangle). LHCA1 is present in smaller complexes in C73 compared to CC-125.

Because of the changes to the PSII bands observed in the BN-PAGE, the interactions between PSII and LHCII were also examined. When the 2D transfers were probed with antibodies raised against the PSBA protein, a range of complexes were observed (Figure 3.9). In the CC-125 cell samples, the expected 30 kDa PSBA was observed in the BN-PAGE bands attributed to PSII, PSII-LHCII, and in the PSI-LHCII region (Figure 3.9, middle-top image, blue rectangle). Some partially denatured bands were also observed running at about 55 kDa (Figure 3.9, top image, red dashed circle), these are likely PSII cores. In comparison, the C73 sample was missing the largest PSII-LHCII complexes, with a greater abundance of the smallest sized

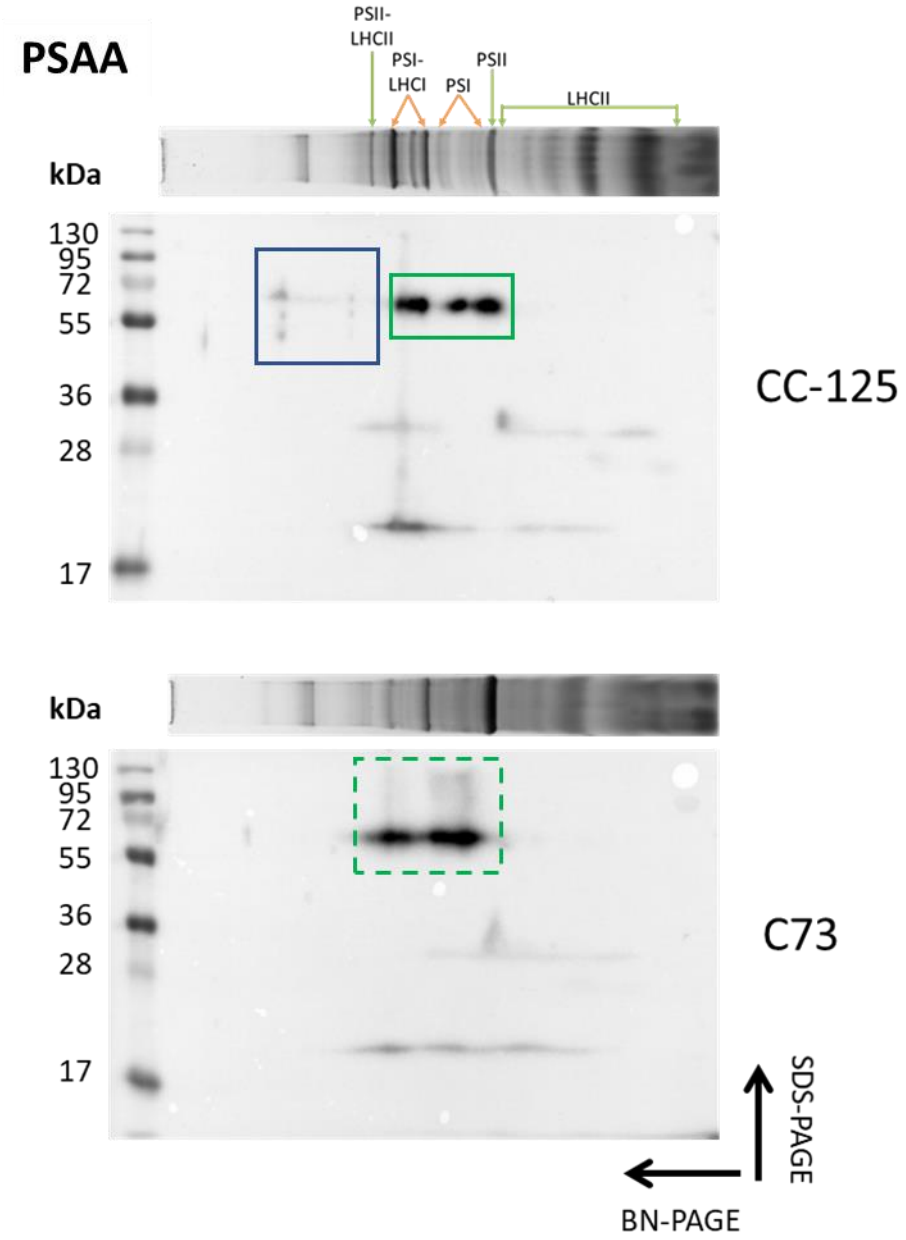

Figure 3.7. Two-dimensional gel electrophoresis to examine the presence of PSI in the large protein complexes. The wild type strain (CC-125), and the strain of interest (C73), were used to compare the presence of the different super complexes of interest.

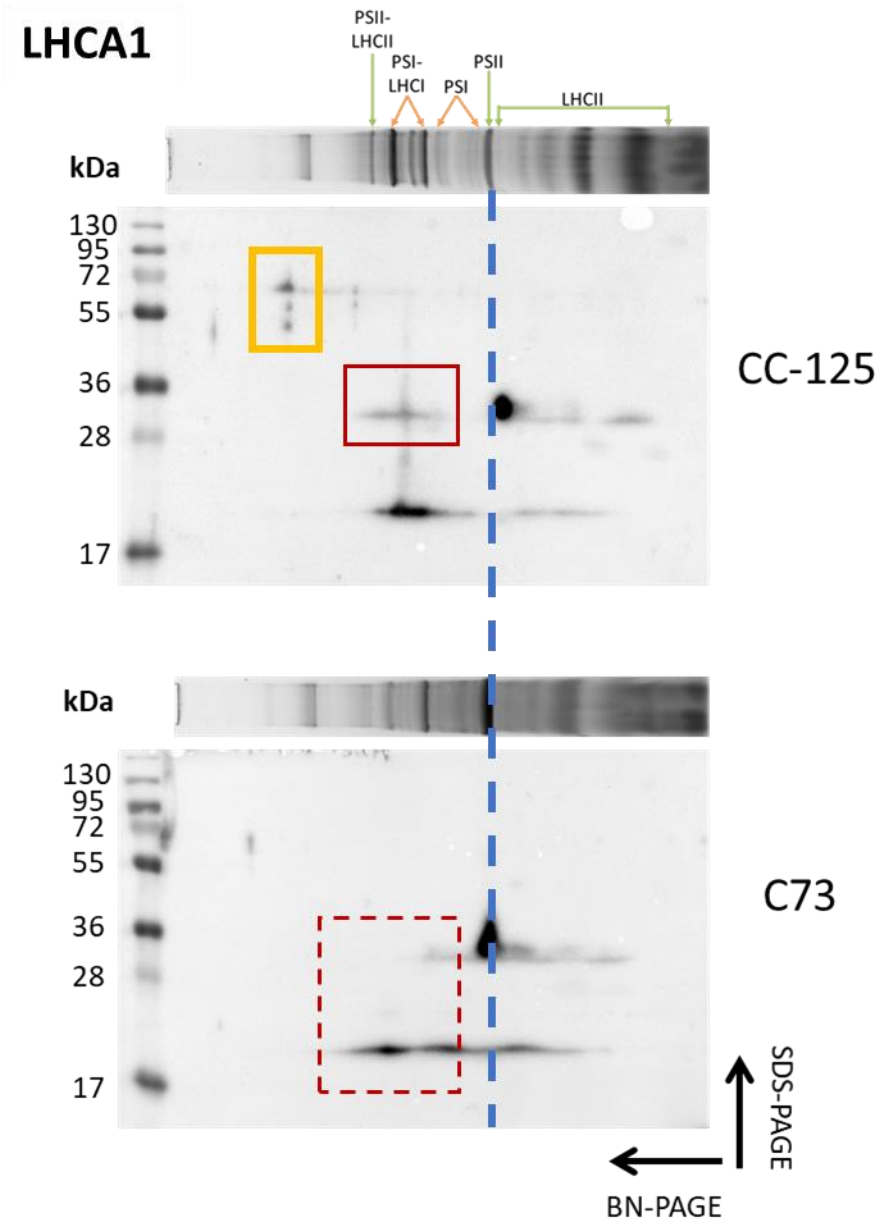

Figure 3.8. Two-dimensional gel electrophoresis analyzes the relative abundance of two different Light Harvesting Complexes. The wild type strain, or CC-125, and the strain of interest, or C73, were used to compare the presence of the different super complexes of interest.

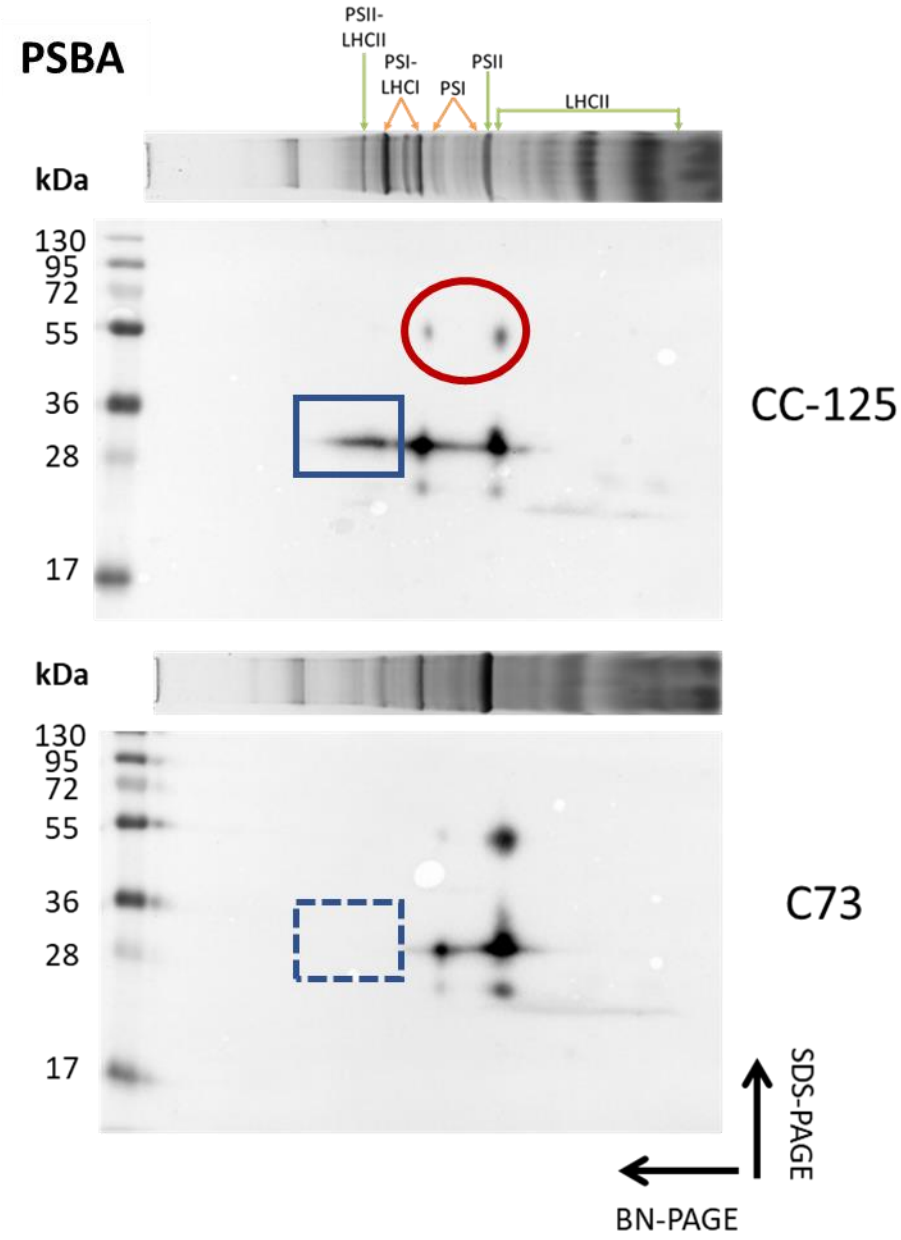

Figure 3.9. Two-dimensional gel electrophoresis to examine the presence of PSII in the large complexes. The wild type strain, or CC-125, and the strain of interest, or C73, were used to compare the presence of the different super complexes of interest.

complexes (Figure 3.9, bottom image, blue dashed rectangle). This conclusion correlates with the results obtained when both the WT and the mutant strains were probed against LHCB2 antibodies (Figure 3.10). One of the most significant differences is the absence in C73 of the 26 kDa band which corresponds to the PSII-LHCII super complex (top image, blue square). The second most observable difference are the strong spots found at 30 kDa and 20 kDa, which correspond with the PSII core (top image, red dashed squares). While in the WT appear as one strong dot and one faint dot, in the C73 strain the two dots can be observed, and one extra band at about 25 kDa (Figure 3.10 bottom image, green dotted circle).

3.6. 77K chlorophyll fluorescence emission spectra

Chlorophyll fluorescence examines the functional connection between LHC antenna proteins, and the reaction centres. Because PSI transfers excitation energy very quickly to examine energy transfer from LHCI to PSI the samples are frozen in liquid nitrogen to a temperature of -196°C (77K). At this temperature, the fluorescence emission from LHCI, PSI, LHCII, and PSII can be separated. Five emission peaks correlate with different parts of the photosynthetic apparatus: 682 nm, 686 nm, 696 nm, 707 nm and 715 nm (Garnier et al., 1986). The peaks recorded at 682 nm and 707 nm correspond to the main LHC antenna in PSII and PSI, respectively (Garnier et al., 1986). The peaks recorded at 696 nm and 715 nm correspond to the cores of both photosystems, respectively (Garnier et al., 1986). To correct for differences in Chl abundance in the samples and the opaqueness of the frozen material, the emission spectra were normalized at 680 nm (the emission value at that wavelength was set to 1, and the rest of the values were divided accordingly). When comparing the normalized spectra of CC-4533 and C73 (Figure 3.11), C73 exhibited decreased fluorescence from PSI and LHCI (707 nm and 715 nm). Because C73 contains the *psaF* mutation I wanted to make sure this difference was not due to that factor. Thus, I also compared C73 to the 3bF strain (Table 2.1). The *psaF* deficient 3bF strain, exhibited notably higher emission in the portion of the spectra corresponding to LHCI and PSI (707 and 715 nm) when compared with C73 (Figure 3.12). The next step to confirm that C73 is lacking a functional arrangement of its LHC would be to clone the gene responsible for the *lgp1* phenotype and understand how it interacts with its PS and LHC proteins, and which other proteins it interacts with.

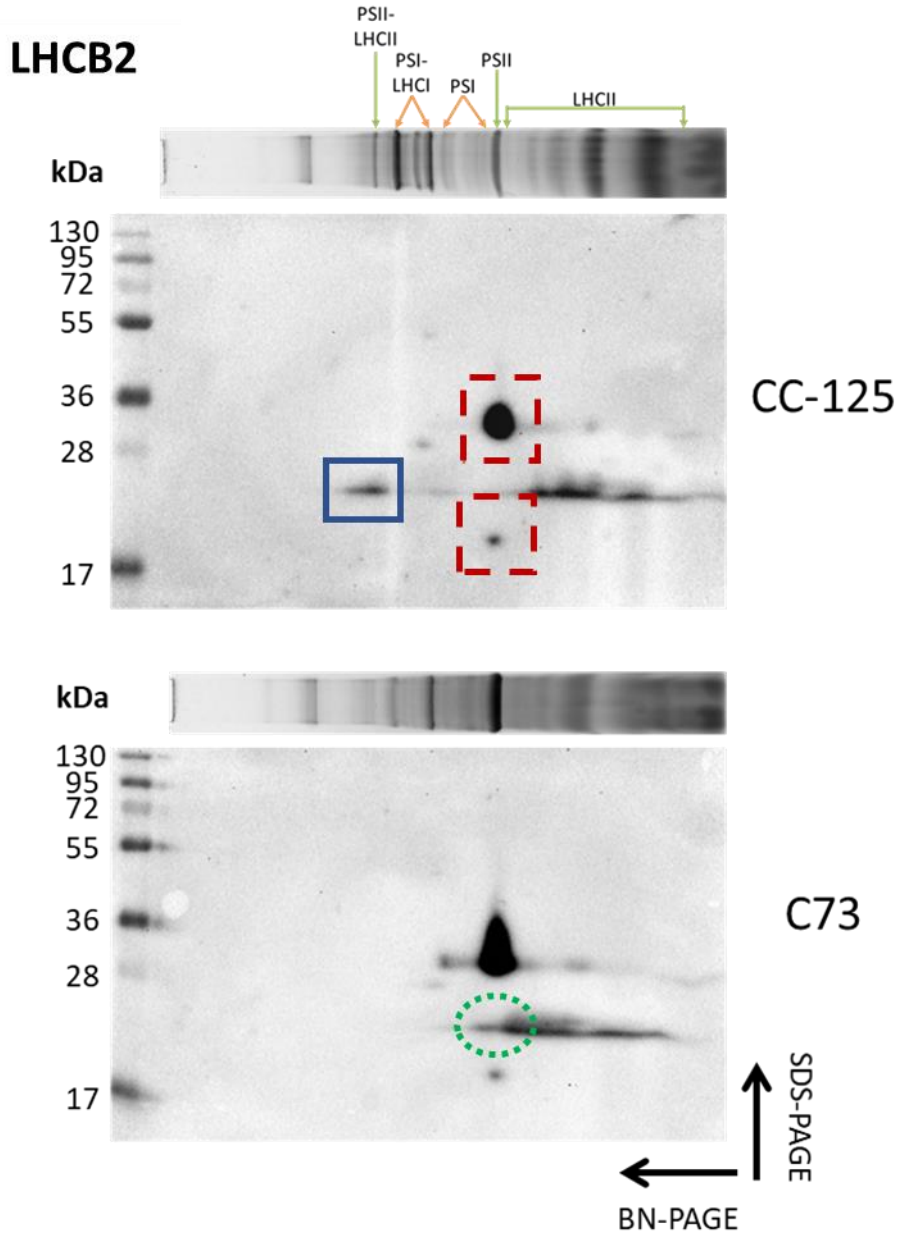

Figure 3.10. Two-dimensional gel electrophoresis to analyze the relative abundance of two different Light Harvesting Complexes in PSII. The wild type strain (CC-125), and the strain of interest (C73), were used to compare the presence of the different super complexes of interest.

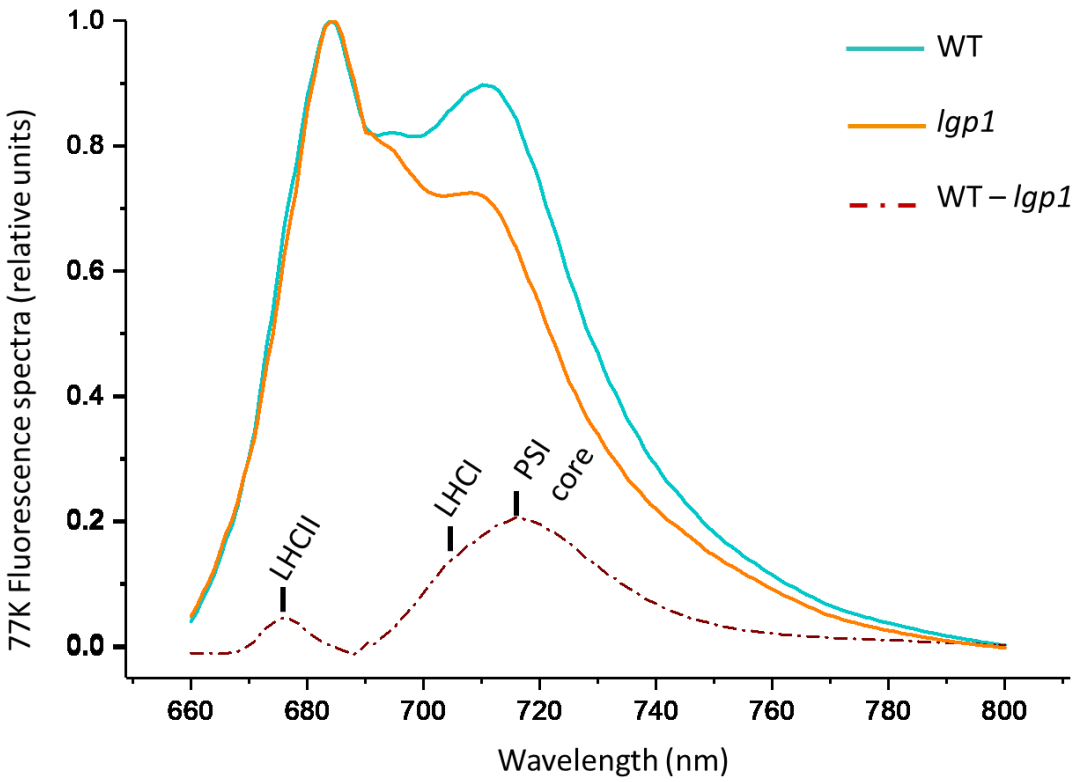

Figure 3.11. Comparison of the normalized 77K fluorescence emission spectra between the CC-4533 (WT) and the mutant strain of interest (C73).

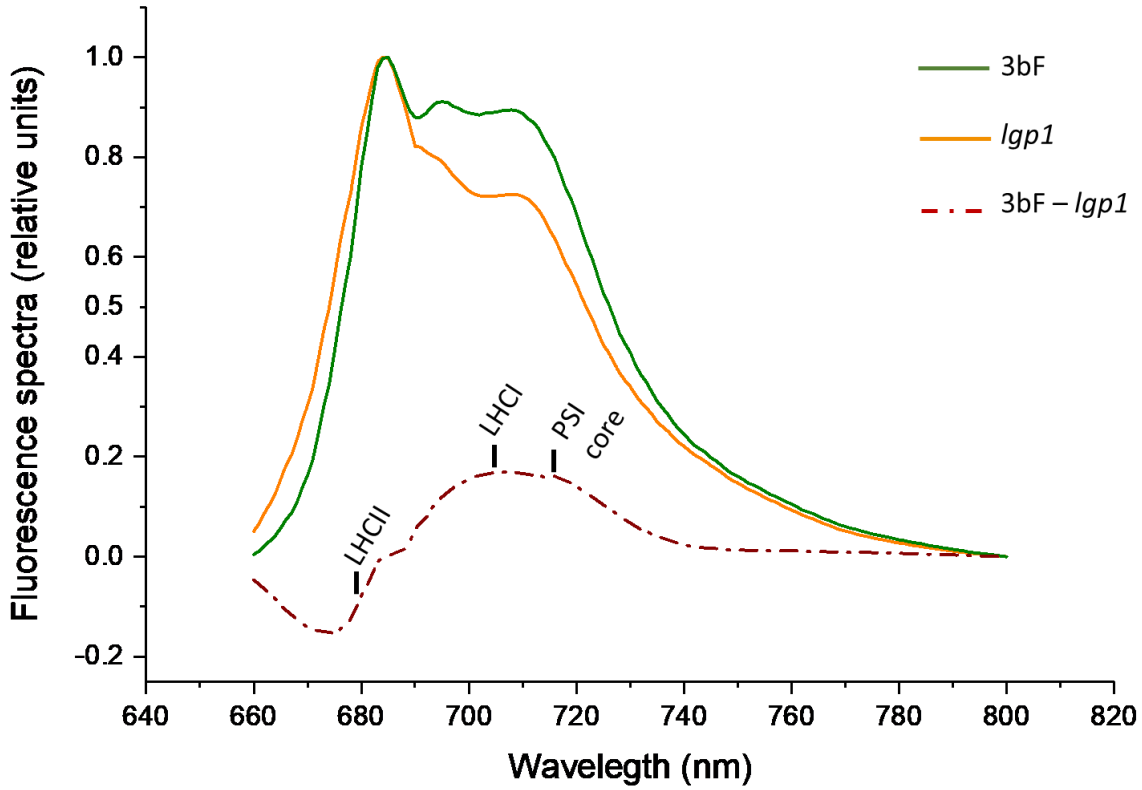

Figure 3.12. Comparison of the normalized 77K fluorescence emission spectra between the 3bF (*psaF*) and the mutant strain of interest (C73).

CHAPTER 4

4. DISCUSSION

The study of the *lgp1* mutant is part of a larger project aimed at examining mechanisms that protect PSI from excess light. One specific aspect of this project was to identify how the LHC proteins are assembled in the thylakoid membrane to modulate the amount of light absorbed. As crystallographic modelling work advances, we have structural information to use in assessing the functional side of LHCA-PSI (Erickson et al., 2015). The *psaF* mutant of *C. reinhardtii* was used as a tool to probe the functional construction of LHCI. The *psaF* mutant is sensitive to high light due to inefficient electron transfer to PSI from plastocyanin (Farah et al., 1995; Hippler et al., 2000). Two previous studies demonstrated the usefulness of the *psaF* mutant for probing PSI photoprotection. Hippler et al., (2000) found that a mutation leading to cells being unable to properly insert light-harvesting proteins into the thylakoid membrane protected *psaF* cells from high light (Hippler et al., 2000). In a similar line, Berry et al., (2011) found that *psaF* cells that contained a mutation in the *STT7 kinase* were also tolerant to high light (Berry et al., 2011). In the case of the *stt7* mutation, cells were unable to undergo state transitions (Berry et al., 2011; Depege et al., 2003). With this block in state transitions, the PQ pool becomes more reduced. However, the LHCB proteins do not transfer to PSI to balance excitation energy across the two photosystems. Thus, PSI is excited to a lesser degree, protecting PSI from light damage. The *lgp1* mutant seems to function in between these two processes. Based on my results, the *lgp1* mutation is a reaction centre-LHC assembly defect that also impacts accumulation of specific LHCA and LHCB proteins.

As I began the project, I tested the C73 strain to ensure it behaved as expected. I grew cells on TAP agar plates under high light, growth light, and in the dark (Figure 3.1). I found that indeed the *lgp1* mutation in the C73 strain suppressed the high-light lethal phenotype of the *psaF* strain (3bf) (Figure 3.1 top left panel). It was also possible to see that the *lgp1* cells had a paler green phenotype compared to the wild type strain (CC-125) but they were darker than the

chlorophyll b deficient CC-1335 strain (Figure 3.1). Thus, I was confident I was working with the correct material and that the C73 phenotype was not the same as that described previously by Hippler et al., 2000 or (Berry et al., 2011).

Based on initial observations of the *lgp1* cells, I hypothesized that the lighter green phenotype of the *lgp1* mutant was caused by lower chlorophyll levels in the cell and, therefore, a decreased capacity for harvesting light. Lower amounts of chlorophyll in the cell should mean lower levels of light harvesting proteins, and decreased excitation of PSI. As suggested in previous reports (Berry et al., 2011; Farah et al., 1995; Hippler et al., 2000) decreased PSI excitation protects the *psaF* mutant and suppresses the high-light lethal phenotype. Essentially, the *lgp1* cells would absorb less light energy at a given Photosynthetic Photon Flex Density (PPFD - μmol photons m^{-2} s^{-1}), and hence survive at a higher PPFD than *psaF* cells that did not have the *lgp1* mutation.

Hippler et al., (2000) described their *psaF* suppressor as having a high Chl a/b ratio (≥8). This generally results in a yellow phenotype as observed in the CC-1355 strain (Figure 3.1 mid-left panel; Chl a/b = 19.2). I had hypothesized that *lgp1* cells had less chlorophyll per cell and likely a higher Chl a/b ratio due to their pale green phenotype. I also expected that this would ultimately be due to diminished LHC protein content in the *lgp1* cells. However, I was surprised to note that the *lgp1* cells exhibited only a small decrease in cellular Chl content and small increase in Chl a/b ratio compared to wildtype cells (Table 3.1).

In higher plants and green algae, chlorophyll can be found bound to both reaction centres and LHC proteins. The photosystems contain only chlorophyll a, while the LHC proteins contain both chlorophyll a and b. Thus, a high Chl a/b ratio suggests fewer LHC per reaction centre. This is clearly observed when examining the CC-1355 cells. They do not produce Chl b, thus they have increased amounts of reaction centre proteins and less LHC proteins when compared to wild type cells on a per membrane protein basis (Figure 3.3-Figure 3.5). Interestingly, the *lgp1* cells had fewer reaction centres and LHC proteins when compared to wild type cells on an equal membrane protein basis (Figure 3.3-Figure 3.5). Looking at the LHCA proteins it appears that those located in the outer ring of the antenna, such as Lhca3, 4, 5, 6 and 9 (Figure 3.4), are impacted to the greatest degree and their location with respect to the PSI reaction centre is highlighted in Figure 4.1.

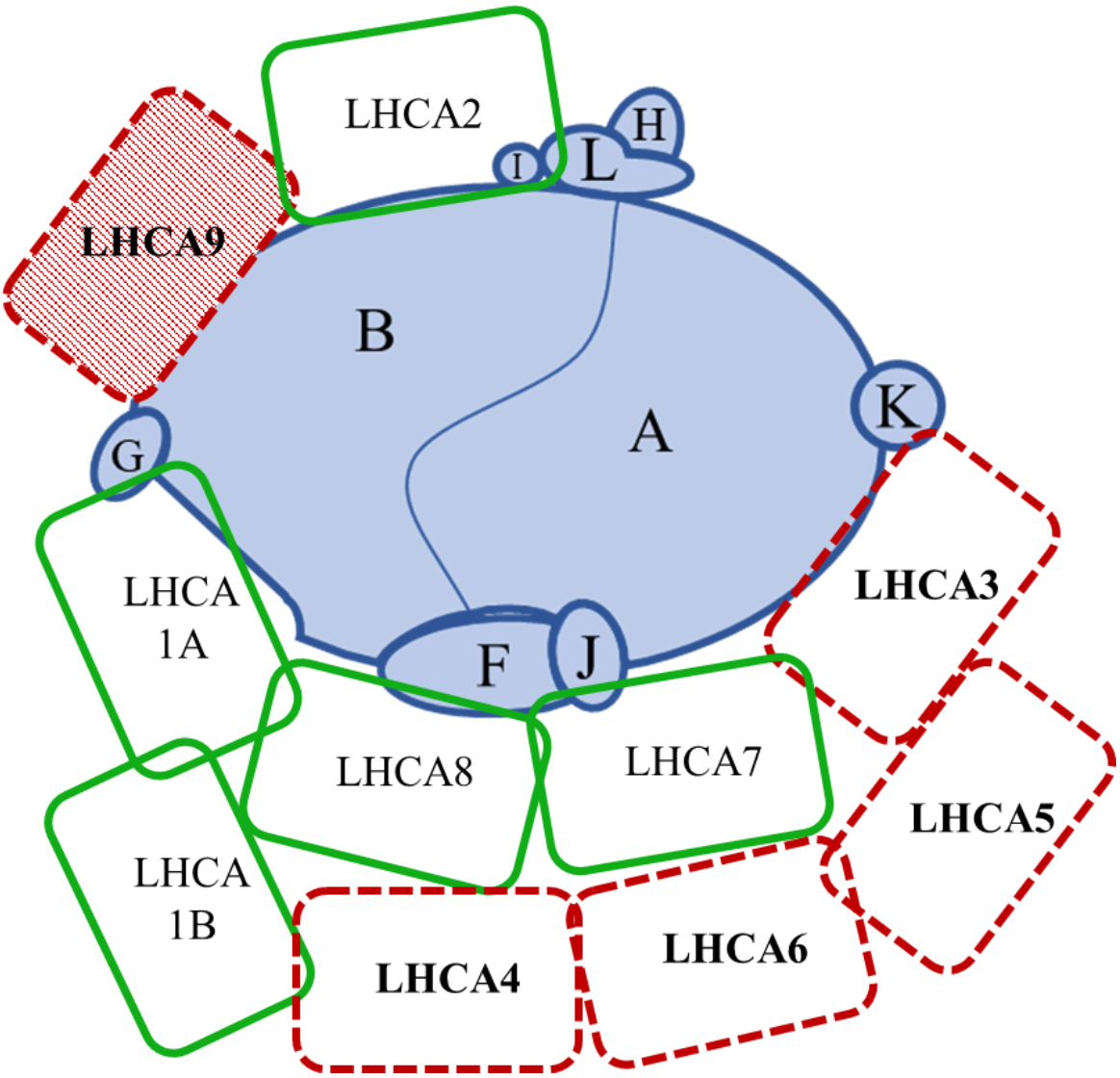

Figure 4.1. Proposed structural distribution of Light Harvesting Complexes surrounding the reaction centre in Photosystem I. The LHCA proteins highlighted in red are those that decrease the most in abundance in *lpg1* (Figure 3.4). Key PSI subunits known to interact with LHCA proteins are shown and denoted by their subunit letter (the gene name would be *PSAA*, for example). This figure is redrawn based on work presented in (Suga et al., 2019).

Similarly, when examining the accumulation of LHCB proteins, only specific subunits of the total studied were impacted by the *lgp1* mutation. LHCB5 is affected the most (Figure 3.5). LHCB5, also called CP26, is located adjacent to the PSII reaction centre core, and it thought to transfer energy from the LHC trimers to CP43 (Sheng et al., 2019). As a monomeric LHCB protein, CP26 is closely related to CP29, which also plays a role in connecting PSII to the larger LHCB trimer antenna. However, we see only a small change in the amount of CP29 (LHCB4) in the immunoblots (Figure 3.5). Interestingly, CP29 was shown to be required for state-transitions (Tokutsu et al., 2009), a process previously shown to impact survival of the *psaF* mutant under high light (Berry et al., 2011). It is also interesting that the C73 cells exhibited only about a 75% decrease in the accumulation of the LHCB trimers (estimated by LHCB2 and LHCBM5 in the immunoblots -Figure 3.4). These proteins, and other that these antibodies are expected to cross react with, form the bulk of the PSII light harvesting antenna. Based on these changes in specific LHC proteins, there appears to be a finer level of control happening, compared to that observed for the CC-1355 strain which simply loses LHC proteins due to the lack of availability of chlorophyll b (Figure 3.3, Figure 3.5).

Based strictly on Hippler et al., (2000)finding that the suppressors they identified all had Chl a/b ratios greater than 8, I looked for a different reason why the high-light lethal phenotype of the *psaF* mutant is suppressed in *lgp1 psaF*. Based on the introductory information it appears that there are large-scale but specific modifications to the LHC systems. Using a BN-PAGE system, I explored the formation of LHC-reaction centre super-complexes in *lgp1* cells I used a BN-PAGE system. This system uses mild detergents on membrane protein complexes. The result is membrane protein complexes that are partially solubilized but remain as super- and mega-complexes that can be resolved in the gel based on their molecular weight (Järvi et al., 2011).

Wild type *C. reinhardtii* cells accumulate large complexes. A commonly observed band at around 1000 kDa is called a C_2S_2 particle (Figure 3.2 and Figure 4.2). The C_2S_2 particle is essentially a dimer containing two copies each of PSII reaction centre core, CP26, CP29, and an LHCII trimer (Iwai et al., 2008; Nield et al., 2000). This band is clearly observed in the BN-PAGE of the WT samples although at a slightly lower than expected molecular weight (Figure 3.6-PSII-LHCII). The C_2S_2 particle band was not observed in either of the *lgp1* or CC-1355 samples (Figure 3.6). We know that this band represents PSII and LHCII in the WT samples

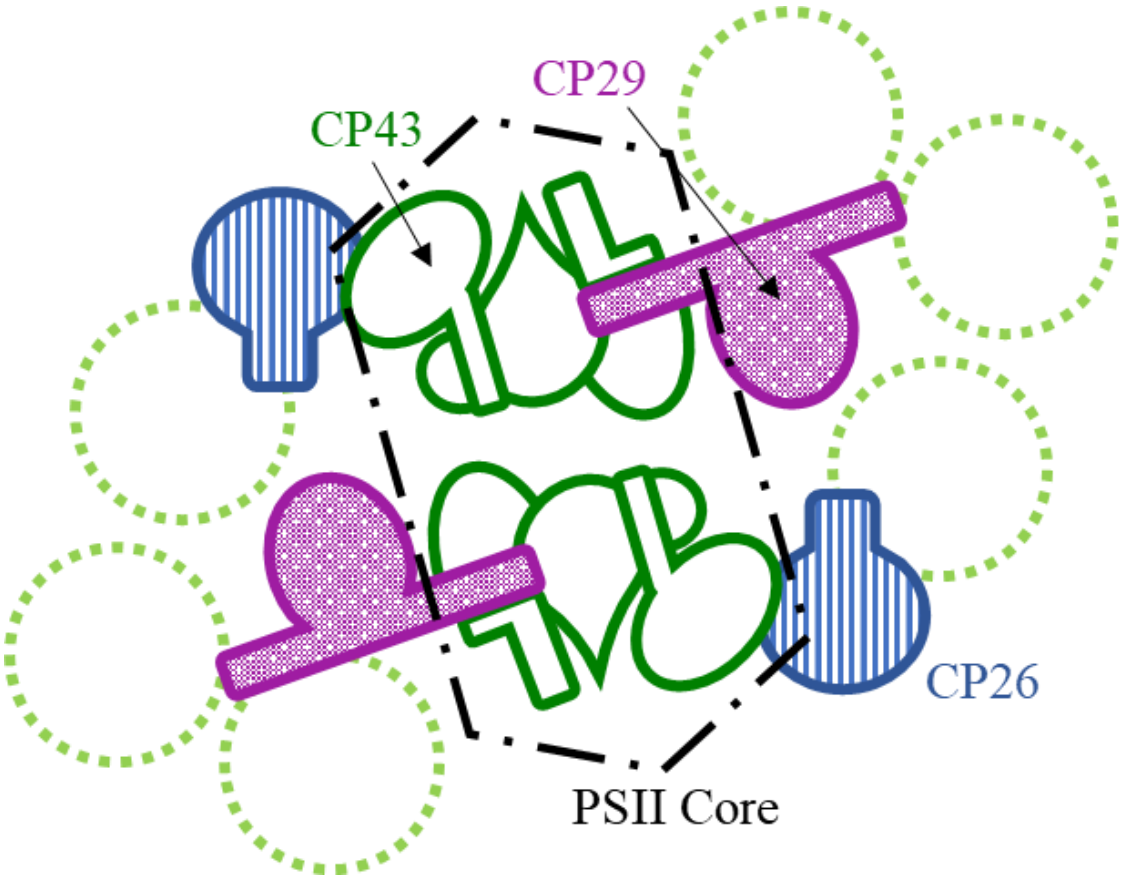

Figure 4.2. Proposed structural distribution of Light Harvesting Complexes surrounding the reaction centre in Photosystem II. In vivo, PSII is thought to form a dimer of reaction centres, surrounded by its light harvesting complex (LHCII). The LHCB proteins affected by the *lgp1* mutation are highlighted in blue (CP26 or LHCB5) and purple (CP29 or LHCB4) (Figure 3.5). LHCB5 is decreased substantially in *lpg1*. The LHCB5 subunit, is thought to form a bridge between the PSII reaction centre at CP43 (PSBC) and a LHCII trimer. This supports energy transfer from the LHCII antenna into the reaction centre and ultimately to P680. Figure is redrawn based on work presented in (Sheng et al., 2019).

based on the 2D-immunoblots using antibodies against the PSII core protein PSBA, and the LHCB2 protein (Figure 3.9 and Figure 3.10). As expected from BN-PAGE the immunoblots failed to detect PSBA or LHCB2 at higher molecular weights in samples from *lgp1* cells. However, there was a concomitant increase in the intensity of the PSII monomer band found at about 350 kDa (Figure 3.6). Thus, it appears that the C73 strain is unable to stably form PSII C_2S_2 complexes.

Similarly, looking at the BN-PAGE results, bands representing PSI-LHCI complexes at around 600 and 720 kDa were missing or much reduced in the C73 and CC-1355 samples (Figure 3.6). There was a slightly lower molecular weight band in all three lanes that may account for some of the missing PSI complexes in the C73 and CC-1355 samples, but I expect that PSI complexes overlap with the PSII band noted at about 350 kDa. This suggestion is supported by the 2D-BN-PAGE immunoblots using antibodies raised against PSAA and LHCA1 (Figure 3.7 and Figure 3.8). Interestingly, looking at the 2D-immunoblots, there are very large PSI-LHC complexes present in the WT samples which are absent in the corresponding C73 samples (Figure 3.7 and Figure 3.8). Plus, I found that the *lgp1* cells accumulated much lower levels of large PSI-LHCI and PSII-LHCII when compared with the wild type cells (Figure 3.6). In fact, despite having more LHC proteins, when *lgp1* samples were run on the BN-PAGE system, they were more similar to CC-1355 cells (Figure 3.6). The results obtained after performing a 2D-PAGE experiment confirmed that *lgp1* cells had a defect in their RCI-LHCI assembly as the signal belonging to those super complexes was not recorded, as shown in Figure 3.7 and Figure 3.8, suggesting that even though lgp1 cells can accumulate all the proteins involved in the photosynthetic apparatus, they are not assembled into functional complexes. As a result, the energy C73 cells receive in their antenna complexes do not efficiently move towards the reaction centres.

Once the assemblage of RC-LHC super complexes was explored and it was concluded to be a defect in the *lgp1* cells, I wanted to examine the *lgp1* LHC functionality *in situ*. A limitation of using BN-PAGE to examine the connection of the LHC antenna to the reaction centres is the isolation process. So, I decided to explore an alternative approach to understand the functional connection between LHC proteins and the reaction centres using chlorophyll fluorescence. I examined the emission spectra emitted by the strains of interest at liquid nitrogen temperature

(77 K). Previous work by Garnier et al., 1986 and Murakami, 1997 showed that the assessment of the presence of photosystems and light harvesting systems and their interactions can be done near-instantaneously when exposing the cells to liquid nitrogen and recording their emission spectra with a spectrofluorometer (Garnier et al., 1986; Murakami, 1997). The CC-4533 strain was my wild type control, while 3bF was the *psaF* mutant sensitive to high light due to inefficient electron transfer to PSI from plastocyanin (Farah et al., 1995; Hippler et al., 2000) (Figure 3.11 and Figure 3.12). This allowed me to compare LHC organization in the *lgp1* cells to the normal (CC-4533) and *psaF* (3bF) cells (Table 2.1). Compared to the WT, the *lgp1* cells showed a diminished PSI-LHCI emission spectra. Lower wavelength correlates with higher energy levels, which could mean that C73 is able to protect its PSI core by rearranging its surrounding LHC. In addition to these observations, I could conclude once more that the *lgp1* cells were different from the *psaF* cells based on the altered PSI fluorescence emission spectra. This higher PSII-LHCII spectra correlates with *psaF* cells not being able to efficiently transfer energy from LHCII to plastoquinone, explaining their sensitivity to high light (Berry et al., 2011; Farah et al., 1995; Hippler et al., 2000).

In conclusion, while the C73 cells containing the *lgp1* mutation are able to grow photoautotrophically under high-light conditions, they exhibit significant defects in the ability to assemble the LHC and reaction centre complexes into functional units. Indeed, this appears to be the mechanism by which the *psaF* high-light lethal phenotype is suppressed in these cells. While I am still working on clearly identifying the gene associated with the *lgp1* mutation, and I need to demonstrate that a cloned gene can rescue the *lgp1* phenotype - restoring full LHC accumulation and assembly, and making C73 cells sensitive to high-light exposure - the phenotype associated with the *lgp1* mutation is quite exciting. The work presented in my thesis represents the first time that a researcher has identified an LHC-RC assembly factor. As researchers have studied large membrane protein complexes, such as PSI and the NDH complex in chloroplasts, and complex I of mitochondria they have observed a common theme. These protein complexes require proteins to help them assemble into their functional complexes. When these support proteins are missing, the larger complexes often fail to accumulate. Based on my results it appears that the LGP1 protein plays a similar role in *C. reinhardtii*. It appears to help bring together and stabilize interactions between the reaction centres and LHC proteins at both PSII and PSI. I find it interesting that in the case of PSI it is the outer ring of LHCA proteins that are most impacted.

While there is much work remaining to fully understand how LGP1 functions, this work represents the crucial first steps in our understanding of how LHC-RC complexes form in photosynthetic eukaryotes.

CHAPTER 5

5. FUTURE WORK AND CONCLUSION

I have strong evidence that the C73 pale green phenotype is linked to the region of chromosome 5 immediately upstream of *PSAD*. However, to confirm that this is indeed the case, I want to clone the gene responsible for the *lgp1* phenotype observed in the C73 cells and use the cloned version to rescue C73 cells. Cloning *LGP1* with an attached epitope tag such as FLAG or a fluorescent protein such as YFP, would allow me to perform subcellular localization studies and detect the fusion protein using commercially available antibodies.

I also do not have a good understanding of how the LGP1 protein interacts with the Photosystem and Light Harvesting proteins. To learn how LGP1 leads to stable RC-LHC interactions, I could use site directed mutagenesis of the LGP1 gene and co-immunoprecipitation to see which other proteins it interacts with, and what parts of LGP1 are critical for that process. Combining the two approaches, I could see what parts of the *LGP1* gene interact with PS and/or LHC proteins. Lastly, 77K fluorescence would also help here, as I could observe when full recovery of LHC-PS functional behaviour is obtained. Using 77K fluorescence and excitation wavelength scanning, it would be possible to determine if different parts of the LGP1 protein are needed to modulate the PSI-LHCA and PSII-LHCB complexes.

5.1. PCR analysis of neighbouring sequenced regions and amplification of *lgp1* region of interest

As mentioned before, the *lgp1* strain was generated by random insertional mutagenesis. The cells were transformed by electroporation using a paromomycin resistance cassette (Berry et al., 2011) and the insertion site was identified using TAIL-PCR (Dent et al., 2015). The *lgp1* mutant was found to have a single insertion, up-stream of the *PSAD* gene on Chromosome V (Figure 5.1, part A). This information was used in designing an approach focused on narrowing and amplifying the region of the chromosome containing the *LGP1* gene (region of interest - ROI).

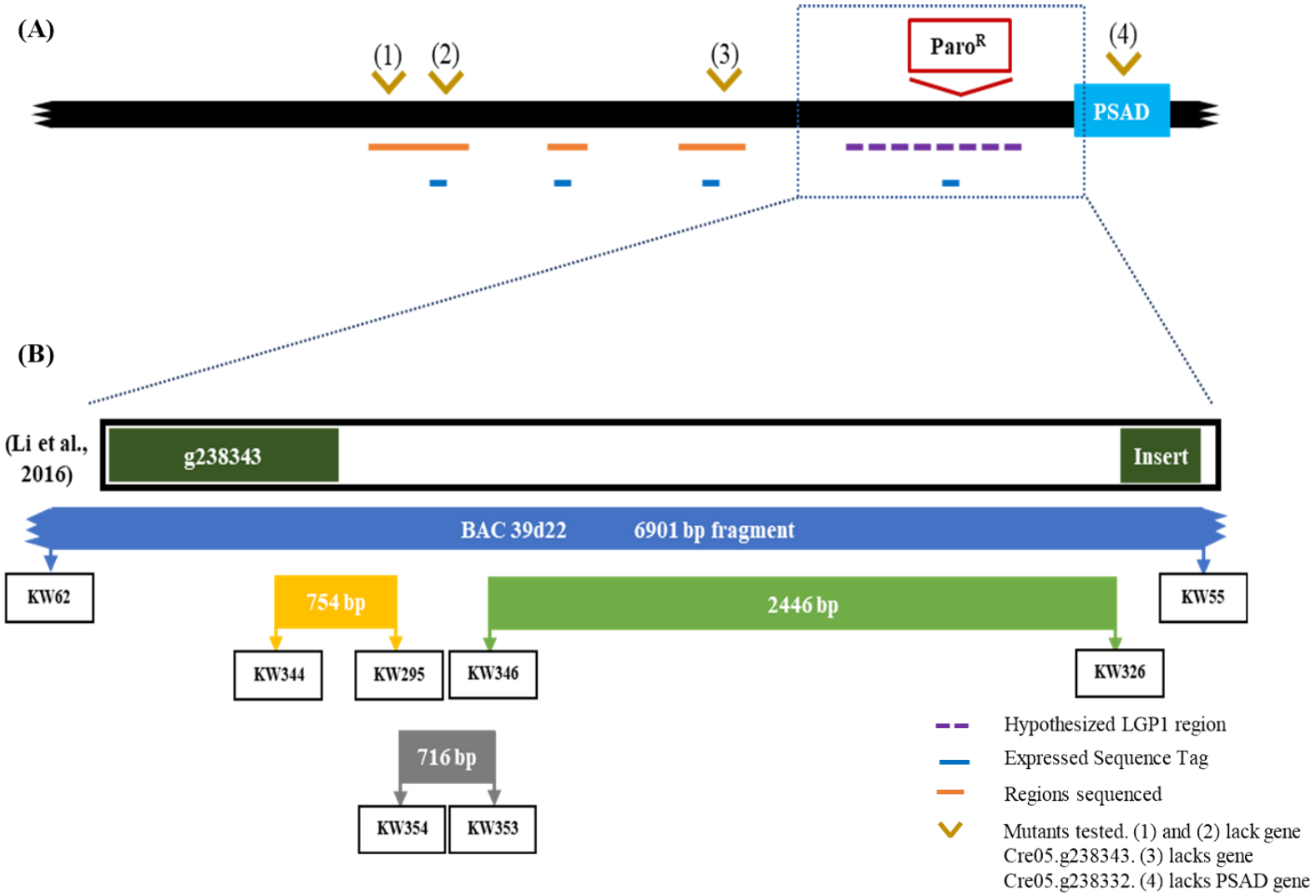

Figure 5.1. Proposed map displaying the genetic approach taken for locating the *LGP1* gene. All the polymerase chain reactions were performed using BAC DNA as a template to amplify the region of interest.

A large-scale functional genomics project using *C. reinhardtii* generated close to 60,000 insertion mutants (Li et al., 2016) which are available to the public through the Chlamydomonas Resource Center. When studying the ROI, three neighbouring genes were found close to the hypothesized LGP1 region: Cre05.g238353, Cre05.g238343 and Cre05.g238332 (*PSAD* gene). These are gene models predicted by the bioinformatics model used on the Chlamydomonas genome. Mutants mapped to these hypothetical genes were ordered from the Chlamydomonas Resource Centre (University of Minnesota, St Paul, MN, USA). Upon growing the strains obtained from the resource center, none of them had the light green phenotype associated with C73. To double check a series of PCR based experiments were performed to test the intactness of these genes in C73 (Table 3.1). Based on PCR analysis all three genes were intact and expressed in the *lgp1* strain, therefore the LGP1 phenotype was due to a different gene, or the bioinformatic models are incorrect. Using the PCR analysis to narrow the location of the *LGP1* gene reduced the focus to a 7 kb region of the genome. I also used immunoblotting analysis to determine whether PSAD protein accumulation was altered in C73 (Figure 3.3). While there was a decrease in PSAD accumulation it was expressed at about 75% of the wild type level.

To increase the ease of amplifying this DNA region, a BAC containing this segment of Chromosome V was obtained from CUGI (Clemson University Genomics Institute). The region of interest was proposed to be about 4 kb pairs (kbp) long. Despite the multiple attempts to amplify it, I was not successful. A different approach was then taken, using three separate PCRs that generated overlapping fragments (Figure 5.1, part B).

5.2. The *LGP1* gene is assembled with the pLM006 plasmid and successfully hosts it

The LGP1 ROI (region of interest) fragments were linked together and cloned into the pLM006 vector using the NEB builder system. This results in the first ATG initiating a potential open reading frame upstream from *PSAD* being cloned in front of the pLM006 *PSAD* promoter (Figure 5.2) for *C. reinhardtii* expression. The pLM006 vector (Figure 2.2) provides Hygromycin resistance to transformed *C. reinhardtii* cells, which is required because the C73 strain already contains a Paromomycin resistance cassette. The presence of LGP1 ROI in pLM006 was confirmed by Sanger sequencing. It will be used to transform C73 and C1 cells in an attempt to rescue the *lgp1* phenotype.

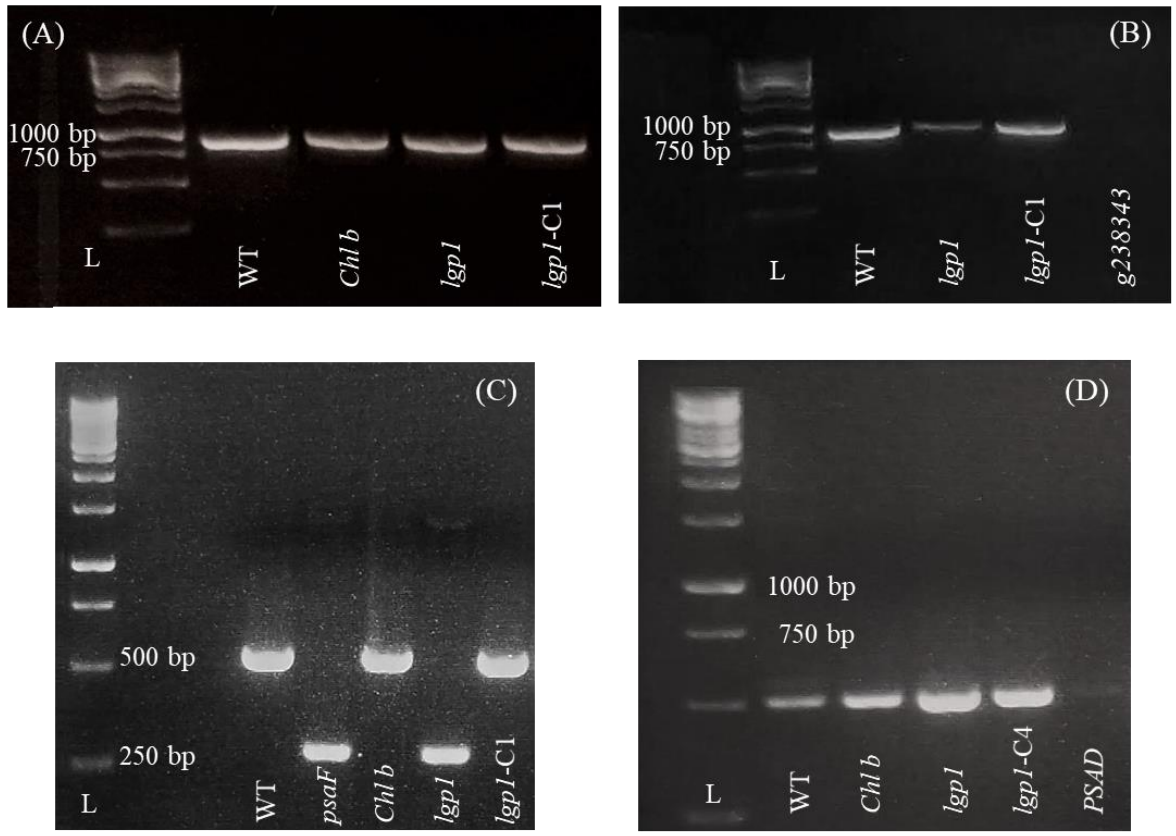

Figure 5.2. Polymerase Chain Reactions on genomic DNA belonging to different mutant strains for confirming the *LGP1* location. **(A)** Gene Cre05.g238353: (1) Ladder, (2) CC-4533 (WT), (3) CC-1355 (*Chl b*), (4) *lgp1*, (5) *lgp1*-C1. **(B)** Finding Cre05.g238343: (1) Ladder, (2) CC-4533 (WT), (3) *lgp1*, (4) *lgp1*-C1, (5) 039260 (g238343). **(C)** Finding *PSAF*: (1) Ladder, (2) CC-4533 (WT), (3) 3bf4c^{-}(*psaF*), (4) CC-1355 (*Chl b*), (5) *lgp1*, (6) *lgp1*-C1. **(D)** Finding *PSAD*: (1) Ladder, (2) CC-4533 (WT), (3) CC-1355 (*Chl b*), (4) *lgp1*, (5) *lgp1*-C4, (6) 139277 *(psaD*).

REFERENCES

Allen, J.F. (2003). State transitions: a question of balance. Science *299*, 1530–1532.

Allorent, G., Tokutsu, R., Roach, T., Peers, G., Cardol, P., Girard-Bascou, J., Seigneurin-Berny, D., Petroutsos, D., Kuntz, M., Breyton, C., et al. (2013). A Dual Strategy to Cope with High Light in Chlamydomonas reinhardtii. Plant Cell *25*, 545–557.

Aro, E.-M. (2004). Dynamics of photosystem II: a proteomic approach to thylakoid protein complexes. J. Exp. Bot. *56*, 347–356.

Bassi, R., Soen, S.Y., Frank, G., Zuber, H., and Rochaix, J.-D. (1992). Characterization of Chlorophylal /bProteins of PhotosystemI from Chlamydomonas reinhardtii". J. Biol. Chem. *267*, 8.

Berry, L.L., Brzezowski, P., and Wilson, K.E. (2011). Inactivation of the STT7 gene protects PsaF-deficient Chlamydomonas reinhardtii cells from oxidative stress under high light. Physiol. Plant. *141*, 188–196.

Camacho-Fernández, C., Hervás, D., Rivas-Sendra, A., Marín, M.P., and Seguí-Simarro, J.M. (2018). Comparison of six different methods to calculate cell densities. Plant Methods *14*.

Dent, R.M., Sharifi, M.N., Malnoë, A., Haglund, C., Calderon, R.H., Wakao, S., and Niyogi, K.K. (2015). Large-scale insertional mutagenesis of *Chlamydomonas* supports phylogenomic functional prediction of photosynthetic genes and analysis of classical acetate-requiring mutants. Plant J. *82*, 337–351.

Depege, N., Bellafiore, S., and Rochaix, J.-D. (2003). Role of Chloroplast Protein Kinase Stt7 in LHCII Phosphorylation and State Transition in Chlamydomonas. Science *299*, 1572–1575.

Du, Z.-Y., Lucker, B.F., Zienkiewicz, K., Miller, T.E., Zienkiewicz, A., Sears, B.B., Kramer, D.M., and Benning, C. (2018). Galactoglycerolipid Lipase PGD1 Is Involved in Thylakoid Membrane Remodeling in Response to Adverse Environmental Conditions in Chlamydomonas. Plant Cell tpc.00446.2017.

Erickson, E., Wakao, S., and Niyogi, K.K. (2015). Light stress and photoprotection in *Chlamydomonas reinhardtii*. Plant J. *82*, 449–465.

Farah, J., Rappaport, F., Choquet, Y., Joliot, P., and Rochaix, J.D. (1995). Isolation of a psaF-deficient mutant of Chlamydomonas reinhardtii: efficient interaction of plastocyanin with the photosystem I reaction center is mediated by the PsaF subunit. EMBO J. *14*, 4976–4984.

Garnier, J., Maroc, J., and Guyon, D. (1986). Low-temperature fluorescence emission spectra and chlorophyll-protein complexes in mutants of Chlamydomonas reinhardtii: Evidence for a new chlorophyll-a-protein complex related to Photosystem I. Biochim. Biophys. Acta BBA - Bioenerg. *851*, 395–406.

Goldschmidt-Clermont, M., and Bassi, R. (2015). Sharing light between two photosystems: mechanism of state transitions. Curr. Opin. Plant Biol. *25*, 71–78.

González-Ballester, D., de Montaigu, A., Galván, A., and Fernández, E. (2005). Restriction enzyme site-directed amplification PCR: A tool to identify regions flanking a marker DNA. Anal. Biochem. *340*, 330–335.

Goodenough, U. (1992). Green yeast. Cell *70*, 533–538.

Gorman, D.S., and Levine, R.P. (1965). Cytochrome f and plastocyanin: their sequence in the photosynthetic electron transport chain of *Chlamydomonas reinhardtii*. *54*, 5.

Green, M.R., Sambrook, J., and Sambrook, J. (2012). Molecular cloning: a laboratory manual (Cold Spring Harbor, N.Y: Cold Spring Harbor Laboratory Press).

Grossman, A.R., Harris, E.E., Hauser, C., Lefebvre, P.A., Martinez, D., Rokhsar, D., Shrager, J., Silflow, C.D., Stern, D., Vallon, O., et al. (2003). *Chlamydomonas reinhardtii* at the Crossroads of Genomics. Eukaryot. Cell *2*, 1137–1150.

Gumpel, N.J., Ralley, L., Girard-Bascou, J., Wollman, F.-A., Nugent, J.H.A., and Purton, S. (1995). Nuclear mutants of Chlamydomonas reinhardtii defective in the biogenesis of the cytochrome b6f complex. Plant Mol. Biol. *29*, 921–932.

Hanks, J.H., and Wallace, J.H. (1958). Determination of Cell Viability. Exp. Biol. Med. *98*, 188–192.

Harris, E.H. (2008). The Clamydomonas Sourcebook: Introduction to Chlamydomonas and Its Laboratory Use. (Burlington: Elsevier).

Hawes, C., and Satiat-Jeunemaitre, B. (2001). Plant cell biology (Oxford University Press).

Hippler, M., Biehler, K., Krieger-Liszkay, A., van Dillewjin, J., and Rochaix, J.-D. (2000). Limitation in Electron Transfer in Photosystem I Donor Side Mutants of *Chlamydomonas reinhardtii*: lethal photo-oxidative damage in high light is overcome in a suppressor strain deficient in the assembly of the light harvesting complex. J. Biol. Chem. *275*, 5852–5859.

Hippler, M., Klein, J., Fink, A., Allinger, T., and Hoerth, P. (2001). Towards functional proteomics of membrane protein complexes: analysis of thylakoid membranes from Chlamydomonas reinhardtii: Towards functional proteomics of membrane proteins. Plant J. *28*, 595–606.

Iwai, M., Takahashi, Y., and Minagawa, J. (2008). Molecular Remodeling of Photosystem II during State Transitions in *Chlamydomonas reinhardtii*. Plant Cell *20*, 2177–2189.

Järvi, S., Suorsa, M., Paakkarinen, V., and Aro, E.-M. (2011). Optimized native gel systems for separation of thylakoid protein complexes: novel super- and mega-complexes. Biochem. J. *439*, 207–214.

Jiang, X., and Stern, D. (2009). Mating and Tetrad Separation of Chlamydomonas reinhardtii for Genetic Analysis. J. Vis. Exp.

Kindle, K.L. (1990). High-frequency nuclear transformation of Chlamydomonas reinhardtii. 5.

Król, M., Ivanov, A.G., Jansson, S., Kloppstech, K., and Huner, N.P.A. (1999). Greening under High Light or Cold Temperature Affects the Level of Xanthophyll-Cycle Pigments, Early Light-Inducible Proteins, and Light-Harvesting Polypeptides in Wild-Type Barley and the *Chlorina f2* Mutant. Plant Physiol. *120*, 193–204.

Li, X., Zhang, R., Patena, W., Gang, S.S., Blum, S.R., Ivanova, N., Yue, R., Robertson, J.M., Lefebvre, P.A., Fitz-Gibbon, S.T., et al. (2016). An Indexed, Mapped Mutant Library Enables Reverse Genetics Studies of Biological Processes in Chlamydomonas reinhardtii[OPEN]. Plant Cell *28*, 367–387.

Li, X.-P., Björkman, O., Shih, C., Grossman, A.R., Rosenquist, M., Jansson, S., and Niyogi, K.K. (2000). A pigment-binding protein essential for regulation of photosynthetic light harvesting. Nature *403*, 391–395.

Lichtenthaler, H.K., and Buschmann, C. (2001). Chlorophylls and Carotenoids: Measurement and Characterization by UV-VIS Spectroscopy. Curr. Protoc. Food Anal. Chem. *1*, F4.3.1-F4.3.8.

Mackinder, L.C.M., Meyer, M.T., Mettler-Altmann, T., Chen, V.K., Mitchell, M.C., Caspari, O., Freeman Rosenzweig, E.S., Pallesen, L., Reeves, G., Itakura, A., et al. (2016). A repeat protein links Rubisco to form the eukaryotic carbon-concentrating organelle. Proc. Natl. Acad. Sci. *113*, 5958–5963.

Mackinder, L.C.M., Chen, C., Leib, R.D., Patena, W., Blum, S.R., Rodman, M., Ramundo, S., Adams, C.M., and Jonikas, M.C. (2017). A Spatial Interactome Reveals the Protein Organization of the Algal CO2-Concentrating Mechanism. Cell *171*, 133-147.e14.

Murakami, A. (1997). Quantitative analysis of 77K fluorescence emission spectra in Synechocystis sp. PCC 6714 and Chlamydomonas reinhardtii with variable PS I/PS II stoichiometries. 8.

Natali, A., and Croce, R. (2015). Characterization of the Major Light-Harvesting Complexes (LHCBM) of the Green Alga Chlamydomonas reinhardtii. PLOS ONE *10*, e0119211.

Nellaepalli, S., Ozawa, S.-I., Kuroda, H., and Takahashi, Y. (2018). The photosystem I assembly apparatus consisting of Ycf3–Y3IP1 and Ycf4 modules. Nat. Commun. *9*.

Nield, J., Funk, C., and Barber, J. (2000). Supermolecular structure of photosystem II and location of the PsbS protein. Philos. Trans. R. Soc. Lond. B. Biol. Sci. *355*, 1337–1344.

Oessner, J.P., Gillham, N.W., and Boynton, J.E. (1986). The sequence of the chloroplast atpB gene and its flanking regions in Chlamydomonas reinhardtii. Gene *44*, 17–28.

Ort, D.R., and Yocum, C.F. (1996). Oxygenic photosynthesis: the light reactions (Kluwer Academic Publishers).

Peterson, G.L. (1977). A simplification of the protein assay method of Lowry et al. which is more generally applicable. Anal. Biochem. *83*, 346–356.

Polle, J.E.W., Benemann, J.R., Tanaka, A., and Melis, A. (2000). Photosynthetic apparatus organization and function in the wild type and a chlorophyll b -less mutant of Chlamydomonas reinhardtii . Dependence on carbon source. Planta *211*, 335–344.

Porra, R.J., and Scheer, H. (2019). Towards a more accurate future for chlorophyll a and b determinations: the inaccuracies of Daniel Arnon's assay. Photosynth. Res. *140*, 215–219.

Pröschold, T., Harris, E.H., and Coleman, A.W. (2005). Portrait of a Species: *Chlamydomonas reinhardtii*. Genetics *170*, 1601–1610.

Rantala, M., Tikkanen, M., and Aro, E.-M. (2017). Proteomic characterization of hierarchical megacomplex formation in Arabidopsis thylakoid membrane. Plant J. *92*, 951–962.

Rochaix, J.-D. (1995). Chlamydomonas Reinhardtii as the Photosynthetic Yeast. Annu. Rev. Genet. *29*, 209–230.

Rochaix, J.-D. (2002). Chlamydomonas, a model system for studying the assembly and dynamics of photosynthetic complexes. FEBS Lett. *529*, 34–38.

Sambrook, J., and Russell, D.W. (2001). Molecular cloning: a laboratory manual (Cold Spring Harbor, N.Y: Cold Spring Harbor Laboratory Press).

Schägger, H., and von Jagow, G. (1991). Blue native electrophoresis for isolation of membrane protein complexes in enzymatically active form. Anal. Biochem. *199*, 223–231.

Sheng, X., Watanabe, A., Li, A., Kim, E., Song, C., Murata, K., Song, D., Minagawa, J., and Liu, Z. (2019). Structural insight into light harvesting for photosystem II in green algae. Nat. Plants *5*, 1320–1330.

Somers, D.A., Samac, D.A., and Olhoft, P.M. (2003). Recent Advances in Legume Transformation: Table I. Plant Physiol. *131*, 892–899.

Su, X., Ma, J., Pan, X., Zhao, X., Chang, W., Liu, Z., Zhang, X., and Li, M. (2019). Antenna arrangement and energy transfer pathways of a green algal photosystem-I–LHCI supercomplex. Nat. Plants *5*, 273–281.

Suga, M., Ozawa, S.-I., Yoshida-Motomura, K., Akita, F., Miyazaki, N., and Takahashi, Y. (2019). Structure of the green algal photosystem I supercomplex with a decameric light-harvesting complex I. Nat. Plants *5*, 626–636.

Taiz, L., Zeiger, E., Moller, I.M., and Murphy, A. (2015). Plant physiology and development (Sinauer Associates).

Tanaka, A., Ito, H., Tanaka, R., Tanaka, N.K., Yoshida, K., and Okada, K. (1998). Chlorophyll a oxygenase (CAO) is involved in chlorophyll b formation from chlorophyll a. Proc. Natl. Acad. Sci. *95*, 12719–12723.

Tokutsu, R., Iwai, M., and Minagawa, J. (2009). CP29, a Monomeric Light-harvesting Complex II Protein, Is Essential for State Transitions in *Chlamydomonas reinhardtii*. J. Biol. Chem. *284*, 7777–7782.

Wilson, K.E., Ivanov, A.G., Öquist, G., Grodzinski, B., Sarhan, F., and Huner, N.P.A. (2006). Energy balance, organellar redox status, and acclimation to environmental stress. Can. J. Bot. *84*, 1355–1370.